博士論文

Somatic ASXL1 mutations in blood cells promote solid tumor progression

（ASXL1変異を伴う血液細胞が固形腫瘍の発症・進展を促進する）

劉　瀟瀟

Tables of Contents

Abbreviations

CHIP: Clonal hematopoiesis of indeterminate potential

MMTV: mouse mammary tumor virus

PyMT: polyomavirus middle tumor antigen

ASXL1: Additional sex combs-like 1

DNMT3A: DNA Methyltransferase 3 Alpha

TET2: Tet Methylcytosine Dioxygenase 2

ROS: Reactive Oxygen Species

1. Abstract

Clonal hematopoiesis of indeterminate potential (CHIP) is an age-associated phenomenon characterized by clonal expansion of blood cells harboring somatic mutations in hematopoietic genes, including *DNMT3A*, *TET2,* and *ASXL1*. Clinical evidence suggests that CHIP is highly prevalent and associated with poor prognosis in solid tumor patients. However, whether blood cells with CHIP mutations play a causal role in promoting the development of solid tumors remained unclear. Using conditional knock-in mice that express CHIP-associated mutant Asxl1 (Asxl1-MT), I showed that expression of Asxl1-MT in T cells, but not in myeloid cells, promoted solid tumor progression in syngeneic transplantation models. I also demonstrated that Asxl1-MT-expressing blood cells accelerated the development of spontaneous mammary tumors induced by MMTV-PyMT. Intratumor analysis of the mammary tumors revealed the reduced T cell infiltration at tumor sites and programmed death receptor-1(PD-1) upregulation in $CD8^+$ T cells in MMTV-PyMT-Asxl1-MT mice. In addition, I found that Asxl1-MT induced T cell dysregulation, including aberrant intrathymic T cell development, decreased CD4/CD8 ratio, and naïve-memory imbalance in peripheral T cells. These results indicate that Asxl1-MT perturbs T cell development and function, *ASXL1*-mutated blood cells exacerbate solid tumor progression.

2. Introduction

2.1 CHIP: Clonal Hematopoiesis of indeterminate potential

2.1.1 CHIP as the premalignant state of blood cancer.

During human aging, somatic mutations are frequently accumulated in many types of cells. Most of the mutations are usually inconsequential, but some rare mutations in the stem cell fraction can turn into dominant clones and expanded clonally, then eventually cause cancer. In 2014, the John Dick and Ravindra Majeti group reported pre-leukemic hematopoietic stem cells (HSCs) with preleukemic mutations such as mutations in epigenetic modifiers. Their findings well described a model for the clonal origin and evolution of AML: preleukemic stem cells contribute to normal blood development with multiple lineages, and when myeloid cells harbor a selective growth advantage and subsequently gain additional mutations, it can confer full malignant potential and leads to AML over time (Shlush et al., 2014)(Corces-Zimmerman et al.). These findings also indicate a premalignant stage can exist before the progression to hematologic cancer.

Recent whole-genome sequencing studies using DNA from human peripheral blood samples revealed that clonal expansion of hematopoietic cells with acquired somatic mutations is unexpectedly common in healthy aged individuals (Jaisw*al et al., 2014)*. This phenomenon is called clonal hematopoiesis (CH). Although scientists have been using different terminologies to describe the similar states of clonal expansion in the

absence of abnormal hematopoiesis. CH and CHIP broadly refer to the same hematologic process. CHIP is age-related, and the major variants occurred in *DNMT3A*, *TET2*, and *ASXL*, which are also known as epigenetic factors. In most cases, individuals with CHIP will not develop any types of diseases. Still, some with additional canceri-initiating somatic mutations may have increased risk of hematologic cancer, all-cause mortality, and also cardiometabolic disease (Jaisw*al et al., 2014)(Genovese et al., 2014)*.

2.1.2 CHIP and non-hematologic diseases, immune function

Since hematopoietic stem cells (HSCs) can produce all blood cell types, mutations acquired in HSCs can cause phenotypic changes both in the stem cell fractions and immune cells. DNMT3A and TET2 are the most common mutation in CHIP, and both of them are enzymes related to DNA methylation. Studies using mice model and human samples with TET2 and DNMT3A mutations showed the increased expression of chemokines (Cxcl1, Cxcl2) and cytokines such as IL-6 (Cull et al., 2017) (Fuster et al., 2017)(Cook et al., 2019), which likely contributes to the inflammatory environment in the systems (or macrophages). And these inflammatory features in macrophages by CHIP is likely to be the cause of promoting atherosclerosis (Rauch et al., 2018). Furthermore, Tet2 disrupted CAR T cells showed altered central memory T cell phenotypes that result

in improved immunotherapies effect (Fraietta et al., 2018). These findings indicate when CHIP-associated mutation acquired HSC contributes to blood production, those mutations can alter the immune functions that lead to non-hematologic diseases or clinical outcomes of immunotherapy.

Clinical evidence suggests that CHIP is particularly prevalent in solid tumor patients, and its presence has an adverse impact on their overall survival(Coombs et al., 2017). The high frequency of CHIP in solid tumor patients is correlated with primal exposure to anti-cancer therapies and smoking habits(Bolton et al., 2020). CHIP mutations in DNA damage repair genes, such as *TP53, PPM1D, CHEK2*, are frequently found in patients with prior exposure to cytotoxic chemotherapy. Smoking is strongly associated with *ASXL1* mutations(Bolton et al., 2020). Whether the blood cells with CHIP-associated mutations have causal effects in solid tumor progression, as they do in cardiovascular diseases(Jaiswal and Ebert, 2019)(Jaiswal et al., 2017), has been unclear. A previous study using Tet2-deficient mice showed that myeloid cell-specific Tet2-deficiency inhibits melanoma progression(Pan et al., 2017), while other studies showed that Tet2-deficiency in immune cells promotes the growth of hepatoma and lung cancer cells(Li et al., 2020)(Nguyen et al., 2021). Thus, it appears that Tet2-deficient immune cells create pro-tumor or anti-tumor microenvironment in a tumor-type dependent manner.

The role of other CHIP-associated mutations in the development of solid tumors has not been investigated experimentally.

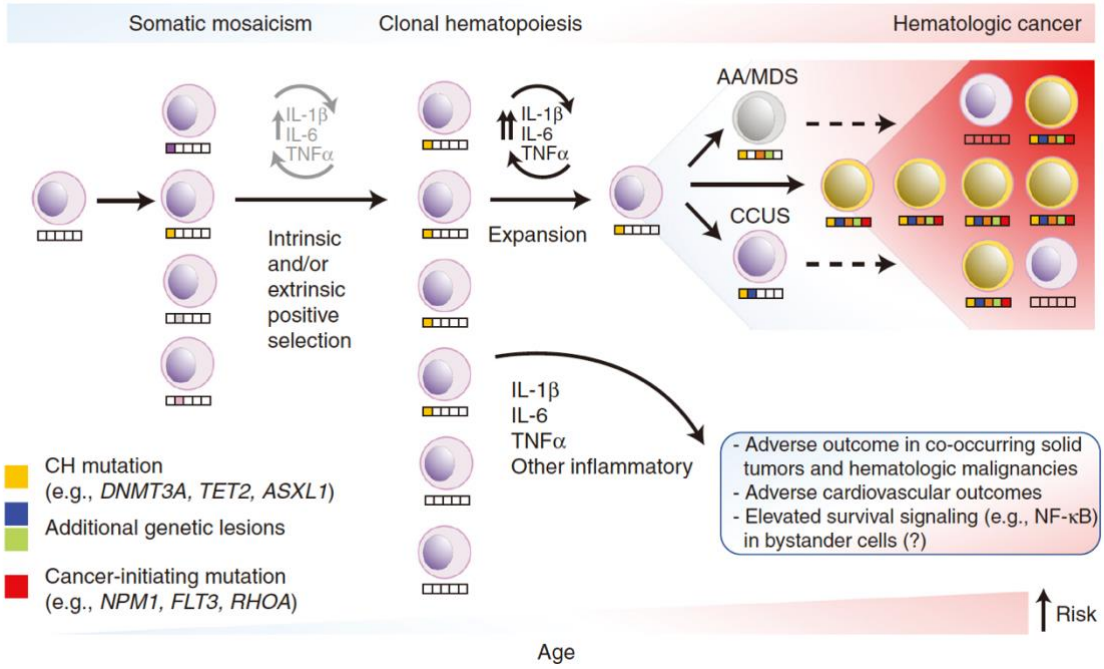

Figure1. Progression from somatic mosaicism through CH into diseases (Kaner et al., 2020). Start from the preleukemic HSC, acquisition of subsequent mutations leads to clonal hematopoiesis, further clonal cytopenia of uncertain significance (CCUS), aplastic anemia (AA), or myelodysplastic syndrome (MDS), and other overt hematologic malignancies such as acute myeloid leukemia. In addition, the inflammatory environment created by CH can also lead to other adverse disease outcomes such as cardiovascular diseases and therapy-related solid tumor patients' survival.

2.2 Somatic ASXL1 Mutations

2.2.1 The role of ASXL1 in hematopoiesis and myeloid malignancies

Additional sex combs-like 1 (ASXL1) is a member of the mammalian ASXL family. ASXL1 regulates gene expression and signal transduction through interactions with multiple proteins, such as BAP1(Asada et al., 2018), EZH2(Inoue et al., 2013), BMI1(Uni et al., 2019), BRD4(Yang et al., 2018), AKT(Fujino et al., 2021),[12,] and NONO(Yamamoto et al., 2021).

Structurally, ASXL1 has an ASX N-terminal (ASXN) domain, an ASX homology (ASXH) domain at the N-terminus region, and a plant homeodomain (PHD) finger at the C-terminal region (Figure 2). The ASXH domain is required for the interaction with BAP1 *(Balasubramani et al., 2015)*. The PHD domain is chromatin and DNA binding module that can recognize different histone methylation subtypes such as H3K4me0 and H3K4me3 (Sanchez and Zhou, 2011). As epigenetic regulators, ASXL1 plays essential role in epigenetic regulation by activating or repressing the transcription genes that effects cell lineage or proliferation. Schermann group showed ASXL1 and BAP1 could form a Polycomb-repressive de-ubiquitinase (PR-DUB) complex. PR-DUB complex can remove monoubiquitin from H2AK119Ub to depress genes catalyzed by PRC (polycomb repressive complex) 1(Scheuermann et al., 2010). Adbel-Wahab group reported that loss of ASXL1 resulted in the global exclusion of H3K27me3 and ASXL1

also bound to components of PRC2 including EZH2 and EED, which indicating ASXL1 cooperate with PRC2 complex to trimethylated H3K27 (Abdel-Wahab et al., 2012).

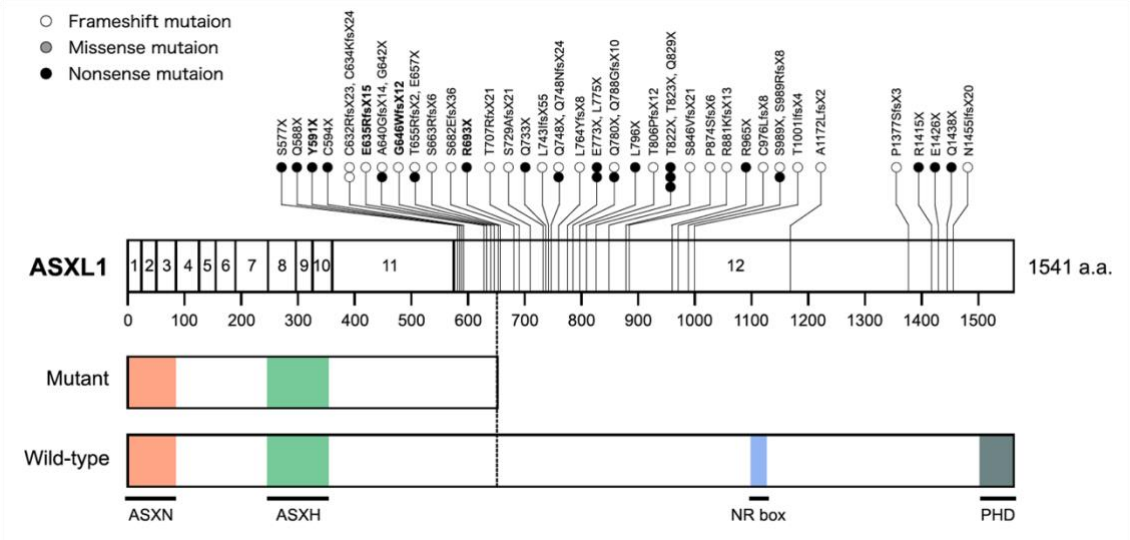

Figure 2. The structure of ASXL1 and the location of ASXL1 mutations in AML patients (Fujino and Kitamura, 2020). Nonsense or frameshift mutations in the ASXL1 gene are concentrated, generating a C-terminally truncated form of ASXL1 (Mutant ASXL1). ASXH is Asx homology; ASXN is Asx N-terminal; NR box is nuclear receptor co-regulator binding motif; PHD is plant homeodomain.

In addition to CHIP, ASXL1 is frequently mutated in all subtypes of myeloid malignancies such as myelodysplastic syndromes (MDS), chronic myelomonocytic leukemia (CMML), myeloproliferative neoplasms (MPN), and acute myeloid leukemia

(AML). ASXL1 mutations are usually associated with poor prognosis (Asada et al., 2019) . Most ASXL1 mutations detected in CHIP and myeloid malignancies are frameshift or nonsense mutation of the last exon that results in C-terminally truncated protein (Bejar et al., 2011). On the other hand, several studies have revealed that ASXL1 mutations provoke malignant transformation through loss of function, dominant-negative , and gain of function mechanisms (Fujino and Kitamura, 2020). The pathogenic ASXL1 mutants alter epigenetic modifications (Abdel-Wahab et al., 2013)(Inoue et al., 2013)(Asada et al., 2019)(Saika et al., 2018), activate AKT/mTOR pathway(Fujino et al., 2021) and disrupt paraspeckle formation (Yamamoto et al., 2021).

2.2.2 ASXL1 mutant Knock in mice: A model mimics human CHIP

Our lab previously established conditional knock-in mice carrying a C-terminally truncated Asxl1 mutant with the floxed STOP cassette under the control of Rosa26 promoter(Nagase et al., 2018). By crossing *Asxl1*-MT KI with Vav-Cre transgenic mice, we can restrict the *Asxl1*-MT expression in the hematopoietic lineage (Vav-Cre *Asxl1*-MT KI). The Vav-Cre-Asxl1-MT$^{fl/fl}$ mice, in which the mutant Asxl1 (Asxl1-MT) was expressed specifically in hematopoietic cells, showed age-related expansion of phenotypic hematopoietic stem cells (HSCs) in native hematopoiesis, which recapitulates

human ASXL1-CHIP. Therefore, I used our conditional *Asxl1*-MT KI mice for studying the mechanism of the mutant ASXL1 acquired blood cells on solid tumor progressions.

2.3 Research purpose

In this study, I aimed to investigate the crosstalk between solid tumors and the blood cells with CHIP-associated ASXL1 mutation and elucidated how blood cells harboring *ASXL1* mutations promote the progression of solid tumors.

3. Materials and Methods

3.1 Materials

3.1.1 Mice

Vav-Cre-*Asxl1*-MT$^{fl/fl}$-KI mice were generated as previously described (Nagase et al., 2018) in our lab. Vav-Cre expresses Cre in hematopoietic cells, endothelial cells, and testes (de Boer et al., 2003) (Joseph et al., 2013). Previously, our lab crossed the conditional *Asxl1*-MT knock-in mice with Vav-Cre transgenic mice to conditional knock in the mutant *Asxl1* in hematopoietic cells. LysM-Cre (C57B/6J background) mice were kindly provided by Prof. Takeharu Sakamoto. LysM-Cre transgenic mice can be used for generating conditional mutations specifically in myeloid cells, including monocytes, mature macrophages, and granulocytes (Clausen et al.). By crossing LysM-Cre mice with conditional *Asxl1*-MT knock-in mice for multiple generations, I generated LysM-Cre-*Asxl1*-MT$^{fl/fl}$-KI to restrict the mutant *Asxl1* only in myeloid lineages for experiments.

Lck-Cre mice were kindly provided by Prof. Yuji Yamanashi. This Lck-Cre expressing Cre under the proximal *lck* promoter in thymocytes (Takahama et al.). By crossing Lck-Cre mice with conditional *Asxl1*-MT knock-in mice for multiple generations, I generated Lck-Cre--*Asxl1*-MT$^{fl/fl}$-KI to restrict the mutant *Asxl1* only in T-cell lineages for experiments.

MMTV-PyMT (C57B/6J background) mice were kindly provided by Prof. Takeharu Sakamoto. MMTV-PyMT transgenic mice the Polyoma Virus middle T antigen (PyMT) under the direction of the Mouse Mammary Tumor Virus (MMTV) promoter (Guy et al., 1992). Hemizygous MMTV-PyMT females can develop palpable mammary tumors with lung/LN metastasis (Fantozzi and Christofori, 2006). By crossing male MMTV-PyMT with female Vav-Cre-*Asxl1*-MT$^{fl/fl}$-KI mice, I generated Vav-Cre-*Asxl1*-MT$^{fl/fl}$-KI-MMTV-PyMT to express the mutant *Asxl1* in hematopoietic cells in MMTV-PyMT mice. Only female Vav-Cre-*Asxl1*-MT$^{fl/fl}$-KI-MMTV-PyMT or control *Asxl1*-MT$^{fl/fl}$-KI-MMTV-PyMT were used for experiments.

All mice were maintained under Specific-Pathogen-Free (SPF) conditions. All animal experiments were performed in accordance with approved protocols from the Laboratory Animal Research Center of The Institute of Medical Science at the University of Tokyo.

3.1.2 Cell line

B16F10 and LLC cells were obtained from the Cell Resource Center for Biomedical Research, Institute of Development, Aging, and Cancer, Tohoku University. MC38 cells were purchased from Kerafast (Boston, MA, USA).

3.1.3 Reagents table

Antibody Name	Clone	Cat#	Maker
CD11b	M1/70	101204	Biolegend
CD11c(p150/90)	N418	13-0114-85	eBioscience
CD19	eBio1D3	13-0193-85	eBioscience
CD4(L3T-4)	GK1.5	13-0041-85	eBioscience
CD8a(Ly-2)	53-6.7	13-0081-85	eBioscience
Gr-1	RB6-8C5	13-5931-85	invitrogen eBioscience
TCR ganma delta		01312D	BD Bioscience Pharmingen
CD49b(integrin alpha 2)	DX5	13-5971-81	invitrogen
Ter119	TER-119	116204	Biolegend
F4/80	BM8	123110	Biolegend
CD8a	53-6.7	100707	eBioscience
CD11b	M1/70	101216	Biolegend
CD25	PC61.5	25-0251-82	eBioscience
CD44	IM7	103011	Biolegend
CD279 (PD-1)	RMP1-30	109109	Biolegend
Ly6C	HK1.4	128014	Biolegend
CD117 (c-Kit)	2B8	17-1171-83	eBioscence
Ly-6G	1A8	127614	Biolegend
B220	RA3-6B2	103222	Biolegend
CD3e	145-2C11	553066	Biolegend
CD4	GK1.5	100438	Biolegend
CD8a	53-6.7	100738	Biolegend
CD45	30-F11	103149	Biolegend
CD366(Tim3)	RMT3-23	119723	Biolegend
CD127	A7R34	135023	Biolegend
CD62L	MEL-14	104407	Biolegend
CD135	A2F10	135305	Biolegend
CD8a	53-6.7	100721	Biolegend
CD4	GK1.5	100411	Biolegend
CD3	17A2	100217	Biolegend
Propidium Iodide Solution		421301	Biolegend
CD16/CD32 Fc Block	2.4G2		BD Pharmingen™

3.2 Methods

3.2.1 Mouse genotyping

Since conditional *Asxl1*-MT-KI mice carrying the 3xFLAG- Asxl1 mutant flox/flox-IRES-EGFP, mouse genotyping can be confirmed with GFP under the existence of Cre recombinase. GFP was detected using the peripheral blood samples from the mice tail and confirmed by flow cytometry. During the establishment of LysM-Cre-*Asxl1*-$MT^{fl/fl}$-KI mice, Lck-Cre-*Asxl1*-$MT^{fl/fl}$-KI mice, and MMTV-PyMT -Vav-Cre-*Asxl1*-$MT^{fl/fl}$-KI mice, genomic PCR was performed to check for, LysM-Cre, Lysm-Cre, and PyMT, *Asxl1*-MT heterozygous (fl/wt) or *Asxl1*-MT homozygous was confirmed by genomic PCR. DNA was extracted from mice tails by the NaOH method. PCR details for each type of mice are written down below (Table 1).

.

Table1 Mouse genotyping details

Type of Mice	Primer	PCR program
Vav-Cre	1) Primer P3: 5'– CATCTGTAGGGCGCAGTAGTC– 3' 2) Primer P4: 5'– CCGTCGTGGTCCTTGTAGTC– 3'	Annealing temperature: 57℃ Cycle: 35
LysM-Cre	1) Primer Rv(WT) : 5'– TTACAGTCGGCCAGGCTGAC– 3' 2) Primer Fw(Common) : 5'– CTTGGGCTGCCAGAATTTCTC – 3' 3) Primer Rv(LysM-Cre) : 5'– CCCAGAAATGCCAGATTACG– 3'	Annealing temperature: 63℃ Cycle: 32
Lck-Cre	1) Lck 5' promoter F primer 25 mer. 5'– CCTTGGTGGAGGAGGGTGGAATGAA – 3' 2) Lck cre-cording R primer 25 mer. 5'– AATGTTGCTGGATAGTTTTTACTGC – 3' 3) Lck 3' cording R primer 24 mer 5'– AGAGCCCTGTTCTGGAAGTTACAA – 3'	Annealing temperature: 60℃ Cycle: 40
MMTV-PyMT	1) PyMT Fw primer: 5'– GGAAGCAAGTACTTCACAAGGG– 3' 2) PyMT Rv primer: 5'– GGAAAGTCACTAGGAGCAGGG– 3'	Annealing temperature: 64℃ Cycle: 35
Asxl1-MT	1) Rosa-GT-FW(common): tcccctcgtgatctgcaactccagtctttc 2) Rosa-GT-Rv(wt): caagcaggagagtataaaactcgggtgagc 3) Neo-5'-Rv (mt): ttgacgagttcttctgaggggatcggcaat	Annealing temperature: 57℃ Cycle: 35

3.2.2 Cell Culture

C57BL/6 derived melanoma B16F10, colon adenocarcinoma MC38 and lewis lung carcinoma LLC cells were cultured in Dulbecco's Modified Eagle Medium (D-MEM, high glucose with L-Glutamine and Phenol Red, FUJIFILM, 044-29765) containing 10% heat-inactivated fetal bovine serum (FBS, F7524, Sigma) and Penicillin-Streptomycin solution (FUJIFILM, 168-23191). For passage, cells were dissociated using Trypsin. All cells were cultured at 37 ℃ with 5% CO_2

3.2.3 Genomic DNA extraction by NaOH

5-8 mm mice tails were cut and collected for DNA extraction. 300ul of 50mM NaOH was added to each tail sample and boiled at 100℃ for 15 minutes. Then added 50ul 1M Tris HCl (PH=8.0) to each sample and vortex well. Centrifuge samples at 12000 rpm speed for 10 minutes. The supernatants were used for PCR.

3.2.4 Syngeneic transplantation model

4×10^5 B16F10, LLC, or MC38 suspended in PBS were subcutaneously injected into the flank of mice per site (two sites in each mouse), under general anesthesia with isoflurane (3%×2 ml/hr for induction and 2%×1.5 ml/hr for maintenance). The hair of the flank area

of the mice was removed before injection. Long-axis (L) and short-axis (S) of the tumors were measured every two days starting from day 6 or day 7 to 14-16 days (B16F10 and LLC) or 21-26 days (MC38) until the tumor volume grew over 800 mm^3. The tumor volume (mm^3) was calculated by the formula $V=L^2\times S\times(\pi/6)$. Tumor weights were measured at the endpoint day. 8-14 weeks mice were used for the experiments. All tumor volume measurements were performed in a blind manner.

3.2.5 Mice tissues processing

For endpoint analysis of tumor models, mice blood biopsies were collected from retro-orbital sinus using heparinized capillary tubes (HIRSCHMANN, #9100275), and mice were immediately sacrificed after the bleeding procedure. Solid tumors were carefully separated from the skin using curved mayo scissors.

For T cells analysis, the spleen and thymus were isolated from the mice then put into FACS buffer (containing 3% FBS and ×1 Penicillin-Streptomycin in PBS). Spleen or thymus was crushed above the 100um cell strainer (Greiner Bio-One, # 54200) with the head of the sterilized 2.5ml syringe plunger, and the dissociated cells were collected for experiments. All red blood cells were lysed with 1×RBC lysis buffer.

3.2.6 Tumor dissociation

Solid tumor-bearing mice were sacrificed at the endpoint day. The tumor tissues were separated carefully from the skin lesions and kept in cold FACS buffer. Enzyme mix was prepared at the time of use. A 2.5ml mix was used for dissociation of tumors that weighted less than 500 mg, and a 5ml mix was used for those that weighed over 500mg. The compositions of the enzyme mix (from Tumor Dissociation Kit, mouse (#130-096-730)). Tumor samples were cut into small pieces with scissors inside the gentleMACS™ C Tubes (#130-093-237) containing the enzyme mix. Dissociation was performed using the gentleMACS Octo Dissociator with Heaters. 37C_m_TDK_1 program was used for soft/medium tumors such as melanoma B16F10 or colon carcinoma MC38. 37C_m_TDK_2 program was used for tough tumors such as breast cancer derived from the MMTV-PyMT model. When the program was finished, 10 ml FACS buffer was added into the C tubes, and the reaction liquid was filtered through a 40-um cell strainer (#542040, Greiner Bio-one). After red blood cell lysis, the dissociated samples were counts for cell numbers and performed for flow cytometric staining.

3.2.7 Spontaneous tumor model assessment

Mice were examined once a week after their age of 8-11week since B6 background

MMTV-PyMT has delayed tumorigenesis than the commonly used FVB background (Davie et al., 2007). and recorded for palpable lumps for tumor-free survival tracing. At the endpoint, mammary tumors/glands were collected from the MMTV-PyMT and Vav-Cre-MMTV-PyMT mice. The numbers of developed tumors (visible and palpable) in the cervical, thoracic, abdominal-inguinal mammary gland were counted were extirpated, and weighed for the whole-body tumor weights. Then the samples were fixed and preserved in formalin for H&E and IHC staining. The tumor infiltrated immune cells were also examined by using flow cytometry.

3.2.8 In vitro T cells culture

Mice splenocytes were collected and stained with biotin antibodies for T cell negative selection after red blood cells lysis. The splenocytes were divided into half and half for CD19, TCRγδ, CD49b, CD11c, B220, Gr1, CD11b, Ter119, CD4 (for CD8 selection), or CD8 (for CD4 selection) staining. Then anti-biotin microbeads (MACS, #130-090-485) and LS columns (MACS, #519091702) were used for selection for CD4 and CD8. After the selection, selected CD4+ and CD8+ cell frequency was confirmed by flow cytometry. 1×10^6 CD4 or CD8 T cells were counted and cultured in non-treated 24 well in the T cell culture mediums (RPMI medium containing 10% FBS, ×1 Penicillin-Streptomycin

solution, murine IL-2 × 30units, and 1/1000 2-ME, the medium need to be freshly made and used within one week). Dynabeads mouse T-activator CD3/CD8 (Gibco^{TM}, #11452D) were used for T cell activation at Day 0 then removed the next day to avoid promotion of the apoptosis of T cell. IL-2 containing medium was changed every other day.

3.2.9 Flow cytometry analysis

For T cells analysis, the spleen and thymus were isolated from the mice and were crushed above the 100-um cell strainer (Greiner Bio-One, # 54200) with the head of the sterilized 2.5ml syringe plunger. For the analysis of tumor infiltrated blood cells, tumors were dissociated (see 3.2.6) and were collected and put into FACS buffer (PBS containing 3% FBS and Penicillin-Streptomycin). Red blood cells were lysed with 1×RBC lysis buffer. 1×10^6 cells per sample were stained with antibodies listed in Table S2. For analyzing the intracellular reactive oxygen species (ROS) levels in T cells, 1×10^6 splenocytes isolated from mice were first stained with surface marker antibodies (PerCP-Cy5.5-CD3, BV421-CD4 and PE-Cy7-CD8), then incubated for 30minutes at 37℃ with 5 μM CellROX Deep Red (Thermo Fisher Scientific, #C10422). For analyzing the mitochondrial membrane potential, 1×10^6 splenocytes were first stained with the surface marker as described in ROS analysis, then incubated with 100 μM MitoTracker Red (Thermo Fisher Scientific,

#M22425). After staining, all cells were washed twice in the FACS buffer and analyzed by FACS AriaIII.

3.2.10 Immunohistochemistry of mice tissues

The murine mammary gland adenocarcinomas, mammary gland contains lumps or lung tissues from MMTV-PyMT and Vav-Cre-MMTV-PyMT were fixed in stocked in 10% formalin-PBS solution. The tissues were embedded in paraffin and processed for sectioning and H&E staining by the Pathology Core Laboratory of the IMSUT.

3.2.11 T-cell Bulk RNA-seq

Murine splenocytes from 12-week Vav-Cre(-) and Vav-Cre (+) Asxl1-MT$^{fl/fl}$ mice were collected and stained with biotinylated antibodies (CD19, TCRγδ, CD49b, CD11c, B220, Gr1, CD11b, Ter119) for T cell negative selection after red blood cells lysis. Then 2-2.5×10^6 CD4$^+$ or CD8$^+$ T cells were sorted by AriaIII. Total RNA was extracted using RNeasy Mini Kit (Qiagen), and the quality and quantity of RNA were checked using Agilent 2100 or AATI and Nanodrop. mRNA was purified from total RNA using poly-T oligo-attached magnetic beads. The library was checked with Qubit and real-time PCR for quantification and bioanalyzer for size distribution detection. Quantified libraries

were pooled and sequenced on Illumina platforms. Pair-end sequencing FASTQ files were aligned to the mouse reference genome (mm10) using HISAT2(Kim et al., 2015) on Galaxy platform(https://usegalaxy.org). Raw gene counts were obtained from read alignments by Rsubread(Liao et al., 2019)(v2.4.3) and further transferred into CPM by edgeR(Robinson et al., 2010) (v3.32.1). After filtering out low-expression genes with CPM lower than 1, all CPM values were log2 transformed for generating unsupervised clustering dendrograms and heatmaps. Differential expression was analyzed with the linear model using limma(Ritchie et al., 2015) (v3.46.0). Genes with FDR<0.05 adjusted by the B-H method were considered as significant differentially expressing genes (DEGs), which were further enrolled in gene ontology analysis using clusterProfiler(Yu et al., 2012)(v3.18.1). For MSigDB gene pathway overlap analysis, DEGs with FDR<0.05 were investigated on http://www.gsea-msigdb.org/gsea/msigdb/annotate.jsp.

3.2.12 Statistic analysis

GraphPad Prism 9 was used to perform statistical analyses. Unpaired student's t-test (two-tailed t-test) and One-way ANOVA was used for pairwise comparisons of significance. The log-rank test. (Mantel-Cox test) was used for the tumor-free survival curve. FlowJo was used for FCM data analysis. The statistical significance (p-value) was indicated in

the figures and figure legends. The p-value (<0.05, <0.01, <0.001) displays as one to three asterisks (*, **, ***). p-values higher than 0.05 were considered as not significant (ns).

4. Results

4.1 Mutant ASXL1 in T cells promotes solid tumor progression in syngeneic transplantation models

I first investigated the influence of blood cells with the *ASXL1* mutation on the growth of solid tumors using the syngeneic mouse tumor models. I crossed Asxl1-MT$^{fl/fl}$ mice with Vav-Cre, LysM-Cre, or Lck-Cre mice to generate the mice expressing Asxl1-MT in all blood cells, myeloid cells, or T cells, respectively. Homozygous (fl/fl) Asxl1-MT mice were identified using PCR and used for experiments (Figure 1A). Expression of GFP (Asxl1-MT) in the myeloid or lymphoid fraction in LysM-Cre or Lck-Cre mice, respectively, was confirmed by FACS (Figure 1B-E).

Next, we subcutaneously injected the C57BL/6 mouse-derived solid tumor cell lines [B16F10 melanoma cells, Lewis lung carcinoma (LLC) cells, and MC38 colon cancer cells] into these mice. The tumor size was measured every other day from day 6 or 7, and the tumor weight was measured at the endpoint day (Figure 2A). We did not observe substantial changes in the growth of all these tumor cells between control and Vav-Cre-Asxl1-MT$^{fl/fl}$ mice, except a slight increase of melanoma weight in Vav-Cre-Asxl1-MT$^{fl/fl}$ mice (Figure 2B). All the tumor cells grew similarly in LysM-Cre-Asxl1-MT$^{fl/fl}$ and control mice (Figure 3). In contrast, the growth of B16F10, LLC, and MC38 cells were all accelerated in Lck-Cre-Asxl1-MT$^{fl/fl}$ mice (Figure 4). These data suggest

that T cell-specific expression of Asxl1-MT promotes solid tumor progression, while expression of Asxl1-MT in other types of blood cells does not.

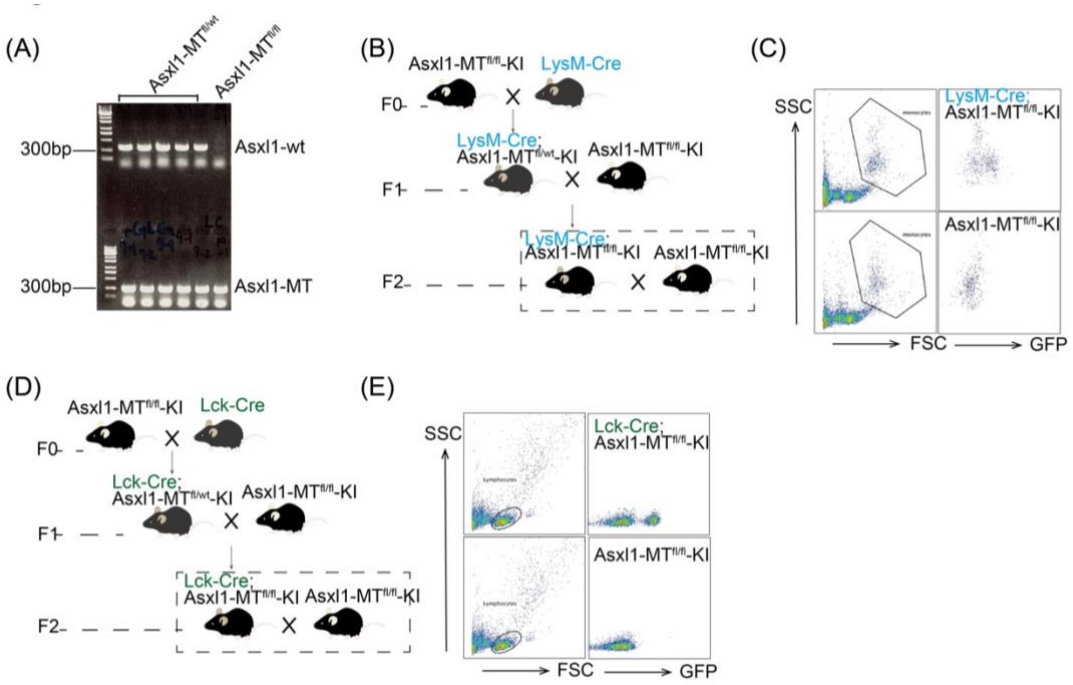

Figure1. Establishment of the LysM-Cre and Lck-Cre conditional Asxl1-MT$^{fl/fl}$ knock-in mice

(A) Representative PCR results for the Asxl1-MT$^{fl/fl}$ and Asxl1-MT$^{fl/wt}$ mice. (**B**) Schematic diagram of establishing LysM-Cre-Asxl1-MT$^{fl/fl}$ knock-in mice. **(C)** The representative FACS plots of peripheral blood in LysM-Cre-Asxl1-MT$^{fl/fl}$ and Asxl1-MT$^{fl/fl}$ mice. GFP expression (= Asxl1-MT expression) was confirmed in myeloid cells. **(D)** Schematic diagram of establishing Lck-Cre-Asxl1-MT$^{fl/fl}$ knock-in mice; **(E)** The representative FACS plots of peripheral blood in Lck-Cre-Asxl1-MT$^{fl/fl}$ and Asxl1-MT$^{fl/fl}$ mice. GFP expression (= Asxl1-MT expression) was confirmed in lymphoid cells.

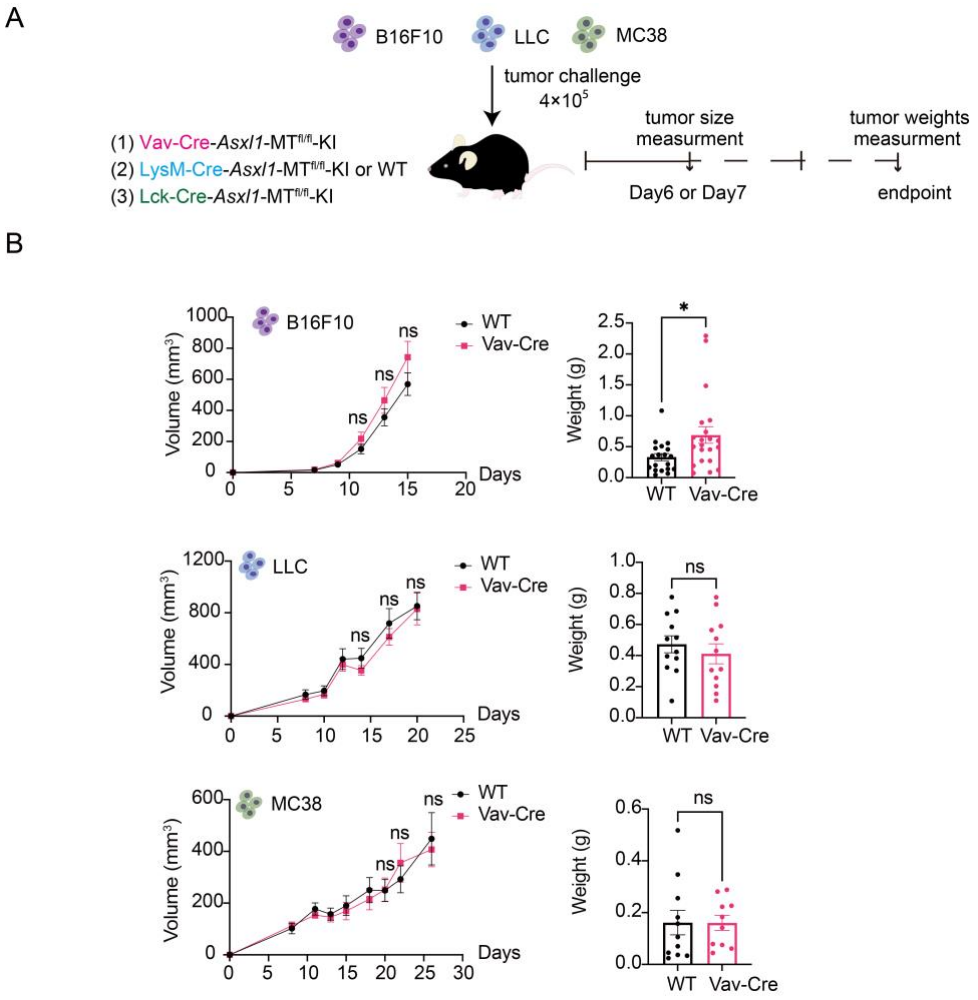

Figure 2. Growth of multiple solid tumors in Vav-Cre-Asxl1-MT$^{fl/fl}$ mice

A. Schematic diagram of the syngeneic mouse models. 4×10^5 of solid tumor cells were subcutaneously injected into mice per site. The tumor volume was measured every other day starting from day 6 or 7. Mice were sacrificed when the tumor volume became over 800 mm^3, and the tumor weights were measured at the endpoint day. Cre(-) and Cre(+) indicate Cre(-/-) and Cre(+/-), respectively.B.The growth curves of tumor volumes (mm^3) and endpoint weights (g) of B16F10 [Vav-Cre(-): n = 33, Vav-Cre(+): n = 26], LLC [Vav-Cre(-): n =12, Vav-Cre(+): n = 12), MC38 [Vav-Cre(-): n = 12, Vav-Cre(+): n = 10] in control and Vav-Cre;Asxl1-MT$^{fl/fl}$ mice. All data are shown as mean ± SEM. Multiple unpaired t-test with Welch correction was used for multiple comparisons of the tumor

volumes. A two-tailed unpaired t-test was used for the comparison of the endpoint weights. Two or three independent experiments using littermate mice were performed in a blind manner. Data are shown as mean ± SEM.

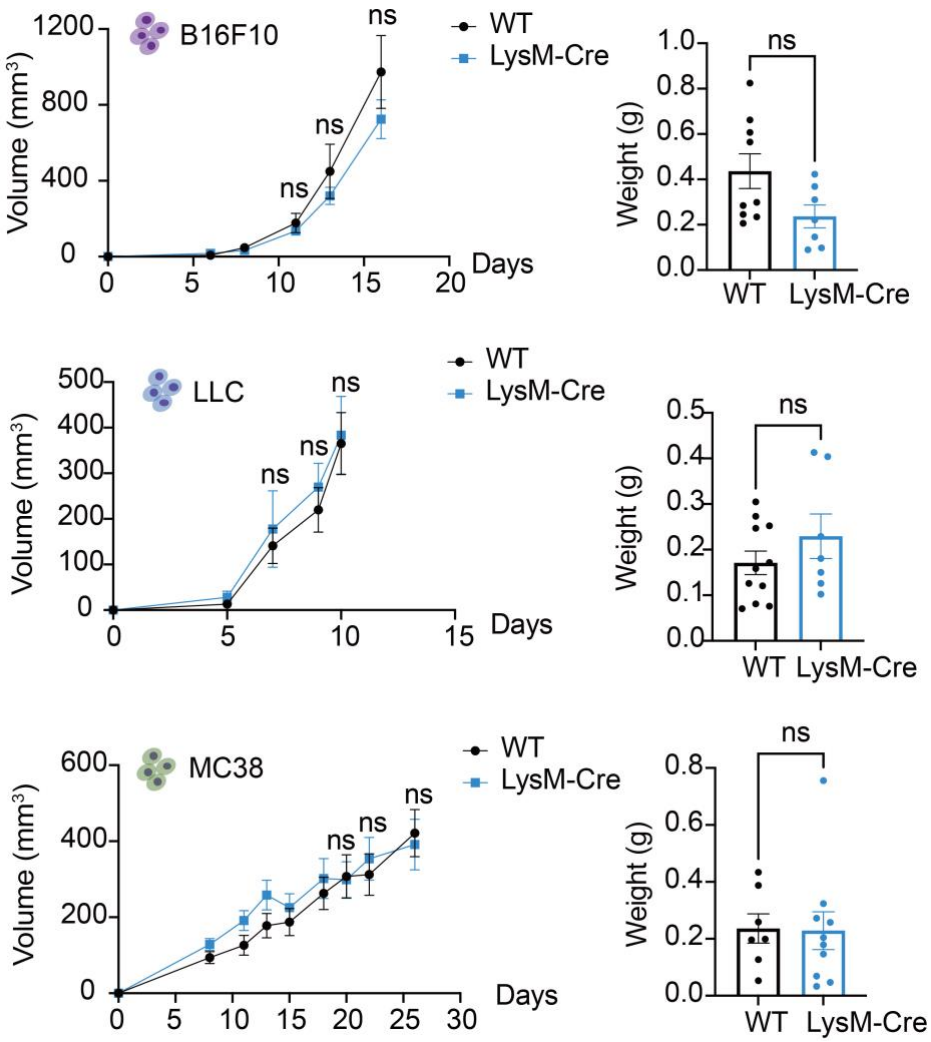

Figure 3. Growth of multiple solid tumors in LysM-Cre-Asxl1-MT$^{fl/fl}$ mice

The growth curves of tumor volumes and endpoint weights of B16F10 [LysM-Cre(-): n = 10, LysM-Cre(+): n =6], LLC [LysM-Cre(-): n =16, LysM-Cre(+): n = 8], MC38 [LysM-Cre(-): n = 7, LysM-Cre(+): n = 11) in control and LysM-Cre-Asxl1-MT$^{fl/fl}$ mice. All data are shown as mean ± SEM. Multiple unpaired t-test with Welch correction was used for multiple comparisons of the tumor volumes. A two-tailed unpaired t-test was

used for the comparison of the endpoint weights. Two or three independent experiments using littermate mice were performed in a blind manner. Data are shown as mean ± SEM.

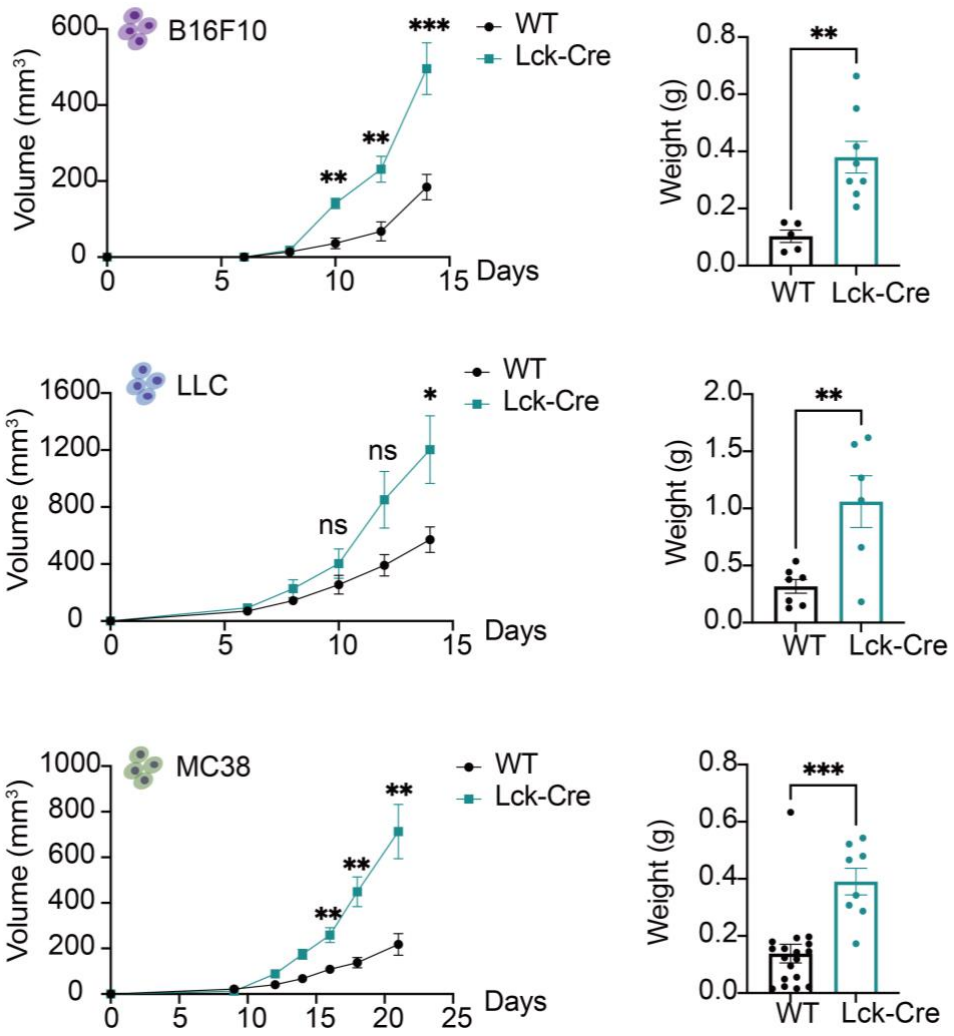

Figure 4. Growth of multiple solid tumors in Lck-Cre-Asxl1-MT$^{fl/fl}$ mice

The growth curves of tumor volumes and endpoint weights of B16F10 [Lck-Cre(-): n = 5, Lck-Cre(+): n = 8], LLC (Lck-Cre(-): n = 7, Lck-Cre(+): n = 6), MC38 (Lck-Cre(-): n = 22, Lck-Cre(+): n = 8) in control and Lck-Cre;Asxl1-MT$^{fl/fl}$ mice. All data are shown as mean ± SEM. Multiple unpaired t-test with Welch correction was used for multiple

comparisons of the tumor volumes. A two-tailed unpaired t-test was used for the comparison of the endpoint weights. Two or three independent experiments using littermate mice were performed in a blind manner. Data are shown as mean ± SEM.

4.2 Expression of mutant ASXL1 in blood cells augments the spontaneous development of mammary tumors in mice

In the syngeneic tumor models, tumors are generated by subcutaneous implantation of established tumor cell lines. Therefore, the models used above do not reflect tumor progression in relevant organ-specific environments. To assess the role of Asxl1-MT expressing blood cells on tumor development in the correct microenvironment, I next used the spontaneous mouse breast cancer model induced by the polyoma middle T antigen (PyMT) driven by the murine mammary tumor virus promoter (MMTV). I crossed Vav-Cre-Asxl1-MT$^{fl/fl}$ mice with MMTV-PyMT mice to generate Vav-Cre; MMTV-PyMT-Asxl1-MT$^{fl/fl}$ mice, in which PyMT and Asxl1-MT were expressed in the mammary gland and blood cells, respectively (Figure 5A-C). Tumor-free survival was assessed by palpation of the mammary glands from the age of 12 weeks. The numbers and weight of the tumors were assessed at the average age of 22 weeks (Figure 6A and Figure 5D). I observed earlier onset of tumors and increased tumor numbers and weights at the endpoint in Asxl1-MT (Vav-Cre-MMTV-PyMT-Asxl1-MT$^{fl/fl}$) mice compared with control (MMTV-PyMT-Asxl1-MT$^{fl/fl}$) mice (Figure 6B-E). Thus, these data suggest that the expression of Asxl1-MT in blood cells creates a pro-tumor microenvironment in the spontaneous breast cancer model. Interestingly, I also found that Asxl1-MT mice developed modest anemia at the endpoint (Figure 6F), which is likely relevant with the

advanced-stage of mammary tumors(Zhao et al., 2018) that developed in Asxl1-MT mice.

Next, I examined the infiltrated immune cells inside the tumors using flow cytometry (Figure 7A-B). The numbers of whole cells per gram in the tumor and the frequency of the infiltrated $CD45^+$ hematopoietic cells did not change between the groups (Figure 8A-B). Importantly, I observed a significant reduction of infiltrated $CD3^+$ and $CD4^+$ T cells in mammary tumors of Asxl1-MT mice (Figure 8C). Although the number of $CD8^+$ T cells was not significantly reduced in tumors of Asxl1-MT mice (Figure 8C), expression of an exhaustion marker PD-1 was upregulated in them (Figure 8D, E). MDSC has the tendency to decrease with no significance (Figure 8F). These data indicate that Asxl1-MT-expressing T cells have an exhausted phenotype and impaired ability to infiltrate the tumor site.

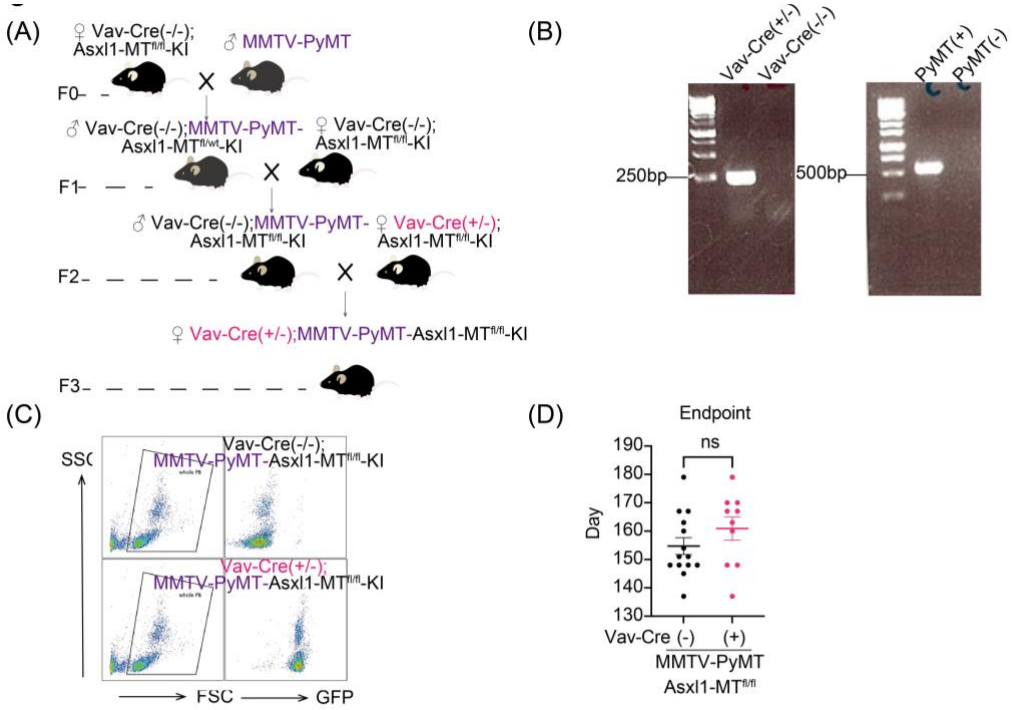

Figure 5. Establishment of the Vav-Cre-MMTV-PyMT-Asxl1-MT$^{fl/fl}$ mice

A. Schematic diagram of establishing Vav-Cre-MMTV-PyMT-Asxl1-MT$^{fl/fl}$ mice. Only female mice were used for experiments. **B.** Representative PCR results for PyMT and Vav-Cre. **C.** The representative FACS plots of peripheral blood of MMTV-PyMT-Asxl1-MT$^{fl/fl}$ and Vav-Cre-MMTV-PyMT-Asxl1-MT$^{fl/fl}$ mice. GFP expression (= Asxl1-MT expression) was confirmed in peripheral blood cells. **D.** The endpoint days of MMTV-PyMT-Asxl1-MT$^{fl/fl}$ [Vav-Cre(-)] and Vav-Cre-MMTV-PyMT-Asxl1-MT$^{fl/fl}$. [Vav-Cre(+)] mice. Vav-Cre(-): n = 14, Vav-Cre(+): n = 10. Data are shown as mean ± SEM. A two-tailed unpaired Mann Whitney t-test was used for the comparison.

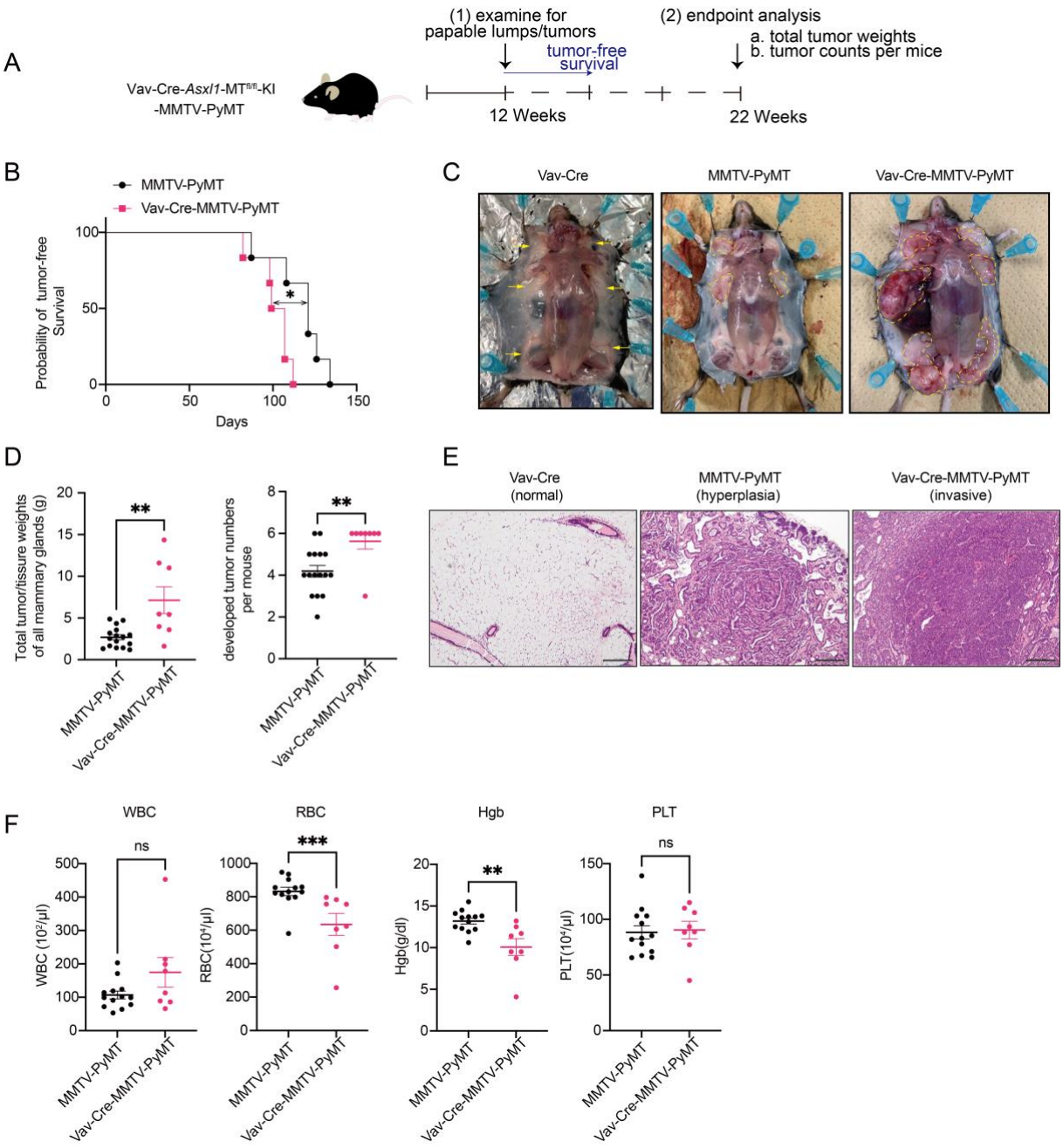

Figure 6. Development of spontaneous mammary tumors was promoted in Vav-Cre-Asxl1-MT$^{fl/fl}$ mice.

A. Schematic diagram of the spontaneous mammary tumor model. Mice were examined once a week from the age of 12 weeks and were considered “tumor-free” until palpable lumps were detected. At the endpoint, all mammary tumors/glands were collected, and

the numbers and weights of developed tumors were assessed. **B.** Tumor-free survival curves of MMTV-PyMT-Asxl1-MT$^{fl/fl}$ (n = 6) and Vav-Cre-MMTV-PyMT-Asxl1-MT$^{fl/fl}$ (n = 6) mice. Log-rank (Mantel-Cox) test was used for comparison. **C.** Representative pictures of the mammary glands. Left: Vav-Cre-Asxl1-MT$^{fl/fl}$ mice; Middle: MMTV-PyMT-Asxl1-MT$^{fl/fl}$ mice; Right: Vav-Cre-MMTV-PyMT-Asxl1-MT$^{fl/fl}$ mice. Yellow arrows indicate mammary glands, and the tumors were circled with yellow dotted lines. **D.** Left: total tumor/tissue weights of all mammary glands per mouse (MMTV-PyMT-Asxl1-MT$^{fl/fl}$: n = 16, Vav-Cre-MMTV-PyMT-Asxl1-MT$^{fl/fl}$: n = 10); Right: numbers of tumors per mouse (MMTV-PyMT-Asxl1-MT$^{fl/fl}$: n = 16, Vav-Cre-MMTV-PyMT-Asxl1-MT$^{fl/fl}$: n = 8). **E.** Representative pictures of HE-staining of the mammary glands in Vav-Cre-Asxl1-MT$^{fl/fl}$ (left), MMTV-PyMT-Asxl1-MT$^{fl/fl}$ (middle), and Vav-Cre-MMTV-PyMT-Asxl1-MT$^{fl/fl}$ (right) mice at day148. The scale bar is 200 μm **F.** Complete Blood Count (CBC) of peripheral blood collected from the mice at their endpoint. WBC: white blood cells; RBC: red blood cells; Hgb: hemoglobin; PLT: platelet. (MMTV-PyMT-Asxl1-MT$^{fl/fl}$: n = 13, Vav-Cre-MMTV-PyMT-Asxl1-MT$^{fl/fl}$: n = 8). Data are shown as mean ± SEM. A two-tailed unpaired Mann Whitney t-test was used for the comparison.

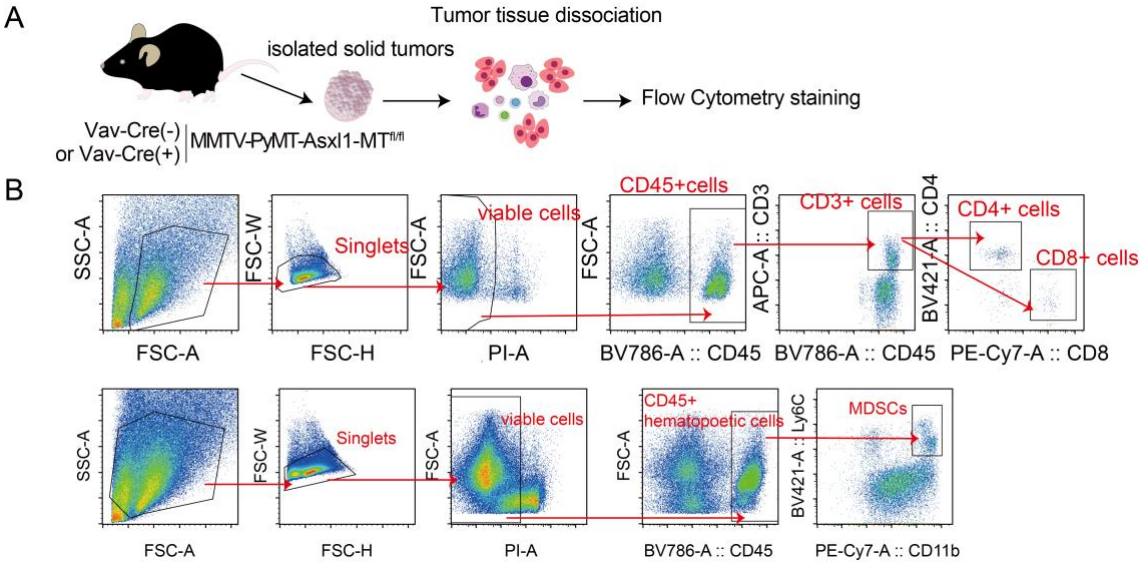

Figure 7. Intratumor analysis in the MMTV-PyMT mice

A. Schematic diagram of intratumor analysis using flow cytometry. Tumors were excised at the endpoint day then Tumors were digested by the tumor dissociator with enzyme cocktails. After RBC lysis of the dissociated samples, cells were stained with antibodies for flow cytometry analysis. **B.** The gating strategy of intratumor T cells. Mammary tumors were collected from the MMTV-PyMT-Asxl1-MT$^{fl/fl}$ [Vav-Cre(-)] mice and Vav-Cre-MMTV-PyMT-Asxl1-MT$^{fl/fl}$ [Vav-Cre(+)] mice.

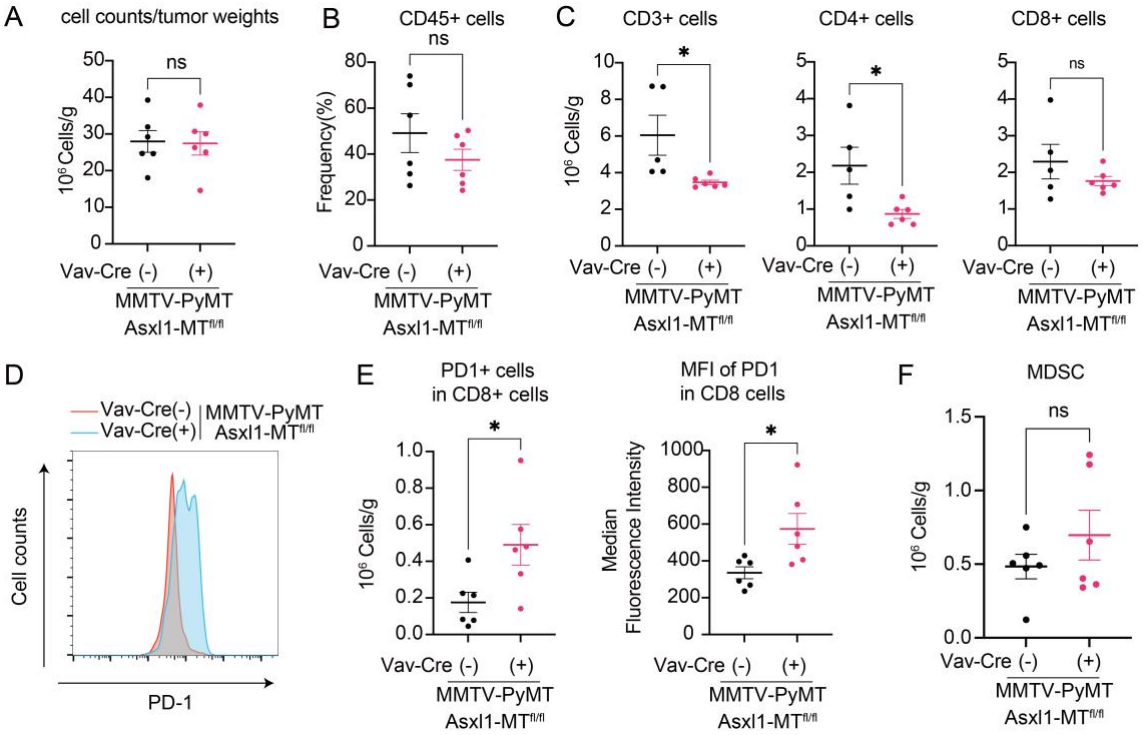

Figure 8. Asxl1-MT-expressing T cells have an exhausted phenotype and impaired ability to infiltrate the tumor site.

Flowcytometry analysis results were shown. **A-B.** Total cell numbers per gram of tumors (**A**), the frequency of infiltrated $CD45^+$ cells (**B**), numbers of tumor infiltrated $CD3^+$, $CD4^+$, $CD8^+$ T cells per gram of tumors (**C**). **D.** Representative FACS plots of PD-1+ in tumor infiltrated CD8+ T cells. **E.** Numbers of tumor infiltrated $PD1^+$ cells in tumor infiltrated CD8+ T cells per gram of tumors (left), and the median fluorescence intensity (right) was shown. **F.** Numbers of tumor infiltrated CD11b+ Ly6C+ Ly6G-MDSC cells per gram of tumors. Data are shown as mean ± SEM. A two-tailed unpaired t-test was used for the comparison.

4.3 Mutant ASXL1 alters T cell development

4.3.1 Mutant ASXL1 alters T cell development in Vav-Cre-Asxl1-MT$^{fl/fl}$ mice

The results described above indicate that Asxl1-MT promotes solid tumor progression through T cell dysregulation. In fact, ASXL1 is highly expressed in mouse and human T cells (Figure 9A, B). To address the effect of Asxl1-MT in T cell development, we first analyzed the number and subset distribution of thymocytes in control and Vav-Cre-Asxl1-MT$^{fl/fl}$ mice. Expression of Asxl1-MT did not change the absolute numbers of thymocytes and the CD4$^-$CD8$^-$ double-negative (DN) fraction (Figure 9C, D). However, the proportion of DN1 cells, especially lineage$^-$c-Kit$^+$ early T-cell precursor (ETP) population, was significantly increased in Asxl1-MT-expressing thymi (Figure 9E). In contrast, CD44$^-$CD25$^+$ DN3 cells were decreased in Asxl1-MT-expressing thymi, indicating a developmental defect from DN1 to later stages (Figure 9F). We also found that the CD8$^+$ single-positive (SP) cells were increased while the CD4$^+$CD8$^+$ double-positive (DP) cells and CD4$^+$ SP cells remained unchanged (Figure 9G). Thus, the expression of Asxl1-MT alters the intrathymic differentiation of immature T cells.

Next, we assessed T cell phenotypes in the peripheral organs. Expression of Asxl1-MT resulted in the decrease of CD4$^+$ cells and the CD4/CD8 ratio in peripheral blood of Vav-Cre-Asxl1-MT$^{fl/fl}$ mice (Figure 10A-B). Intriguingly, we also found a dramatic reduction of naïve CD4$^+$ and CD8$^+$ T cells and an increase of memory and

effector $CD8^+$ T cells in the spleen of Vav-Cre-Asxl1-$MT^{fl/fl}$ mice (Figure 10C-D). The reduction of peripheral naïve T cells with a relative increase of memory/effector T cells are typical immunosenescent features that are observed in aged T cells(Lanzer et al., 2014), (Aiello et al., 2019), (Mittelbrunn and Kroemer, 2021).

Taken together, these data suggest that mutant Asxl1 perturbs T cell development in the thymus and induces naïve-memory imbalance in peripheral organs (Figure 10E).

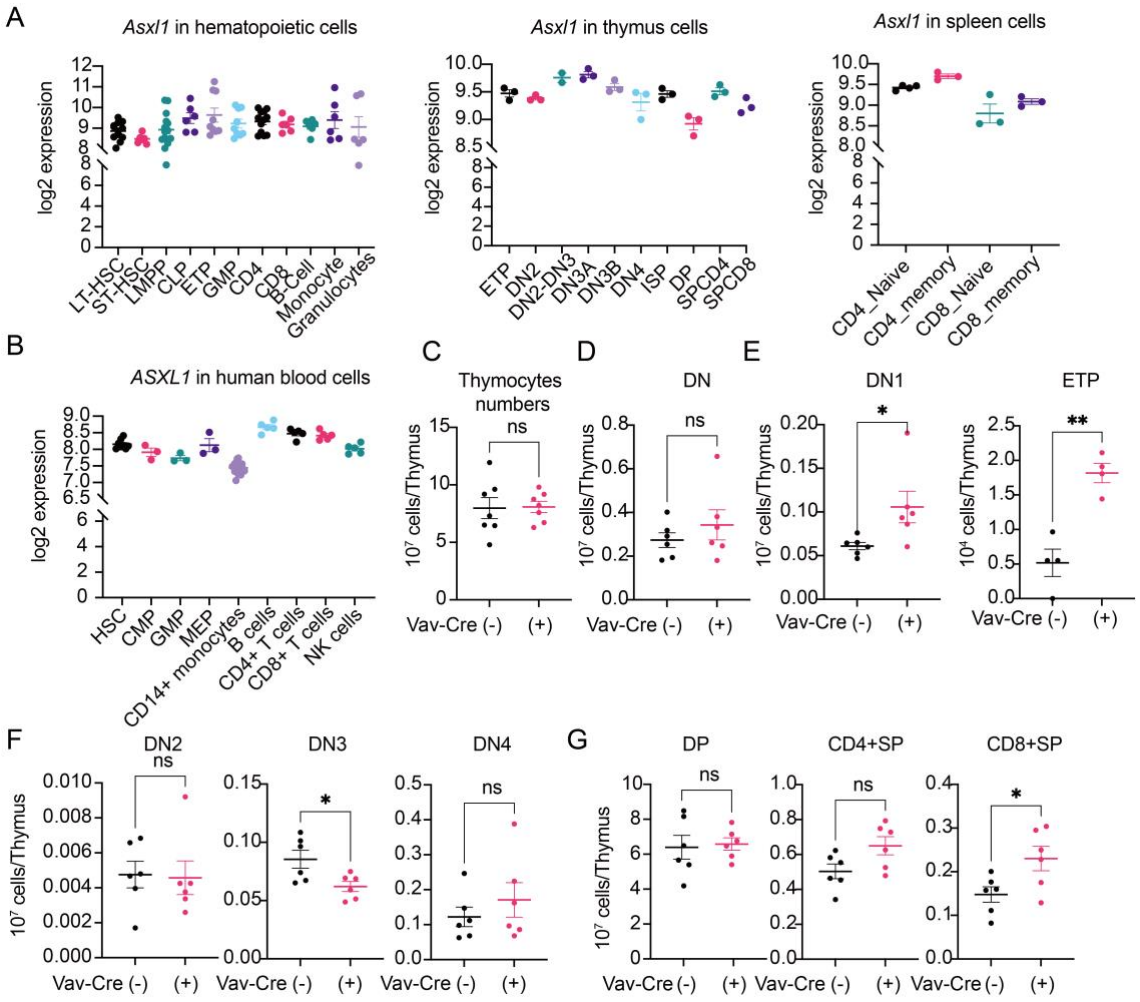

Figure 9. Asxl1-MT perturbs T cell development in the thymus

A, B Log2 expression of murine *Asxl1* in normal hematopoietic cells, thymocytes, and splenocytes. **A** and that of *ASXL1* in human normal hematopoietic cells **B**. Data were exported from the bloodspot website (https://servers.binf.ku.dk/bloodspot/). **C-G** Total numbers of thymocytes (**C**), numbers of $CD4^-CD8^-$ DN cells (**D**), numbers of $CD4^-CD8^-CD44^+CD25^-$ DN1 cells and $Lineage^-CD4^-CD8^-CD44^+$ $ckit^+$ $CD25^-$ ETP cells (**E**), numbers of $CD4^-CD8^-CD44^+CD25^+$ DN2, $CD4^-CD8^-CD44^-CD25^+$ DN3, and $CD4^-CD8^-CD44^-CD25^-$ DN4 cells (**F**), and numbers of $CD4^+CD8^+$ DP, $CD4^+CD8^-$ SP, and $CD4^-CD8^+$ SP cells (**G**) in thymus of Asxl1-$MT^{fl/fl}$ [Vav-Cre(-)] and Vav-Cre;Asxl1-$MT^{fl/fl}$ [Vav-Cre(+)] mice are shown. Data are shown as mean ± SEM. A two-tailed unpaired t-

test was used for the comparison.

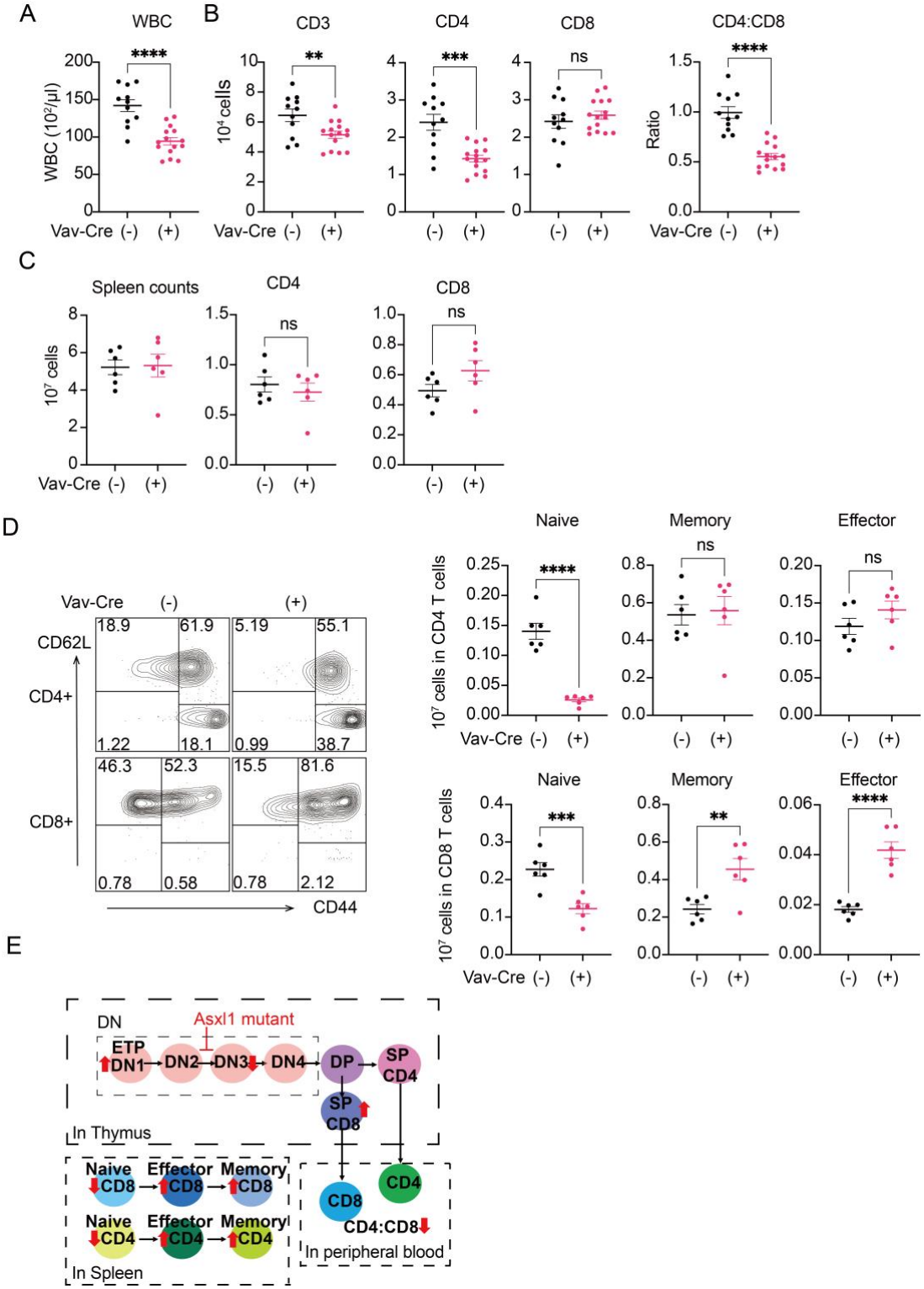

Figure 10. Asxl1-MT perturbs peripheral T cell development and naïve T cell maintenance

A. Complete Blood Count of white blood cells (WBC) in peripheral blood collected from the mice. **B**. Cell counts of $CD3^+$, $CD4^+$, $CD8^+$ T cells and CD4/CD8 ratio in peripheral blood of Asxl1-$MT^{fl/fl}$ [Vav-Cre(-)] and Vav-Cre;Asxl1-$MT^{fl/fl}$ [Vav-Cre(+)] mice are shown. **C**. Cells counts of the whole splenocytes and $CD4^+$ and $CD8^+$ T cells. **D**. Cell counts in $CD4^+$ and $CD8^+$ T cells of naïve ($CD62L^+$ $CD44^-$), effector ($CD62L^-CD44^+$) and memory ($CD62L^+CD44^+$) fractions in spleen. Representative FACS plots (left) and their quantification (right) are shown. Data are shown as mean ± SEM. A two-tailed unpaired t-test was used for the comparison. **E.** The scheme of the effect of Asxl1-MT in thymic and peripheral T cell development.

4.3.1 Mutant ASXL1 alters T cell development in Lck-Cre-Asxl1-MT$^{fl/fl}$ mice

Inside the thymus of Lck-Cre-Asxl1-MT$^{fl/fl}$ mice, I found impaired differentiation of DN3(Double Negative 3) and DN4 (Double Negative 4), DP (Double Positive), SP CD4+ (Single Positive CD4+) and SP CD8+ (Single Positive CD8+) fractions (Figure 11A-C). I also found an evident increased CD8/CD4 ratio in the peripheral blood as the same results in Vav-Cre-Asxl1-MT$^{fl/fl}$ mice (Figure 11D). TCRβ rearrangements occur in DN3 following by a TCR αrearrangements in DP. Therefore, these data suggest that mutant ASXL1 perturbs αβ T cell development in the thymus (Figure 11E).

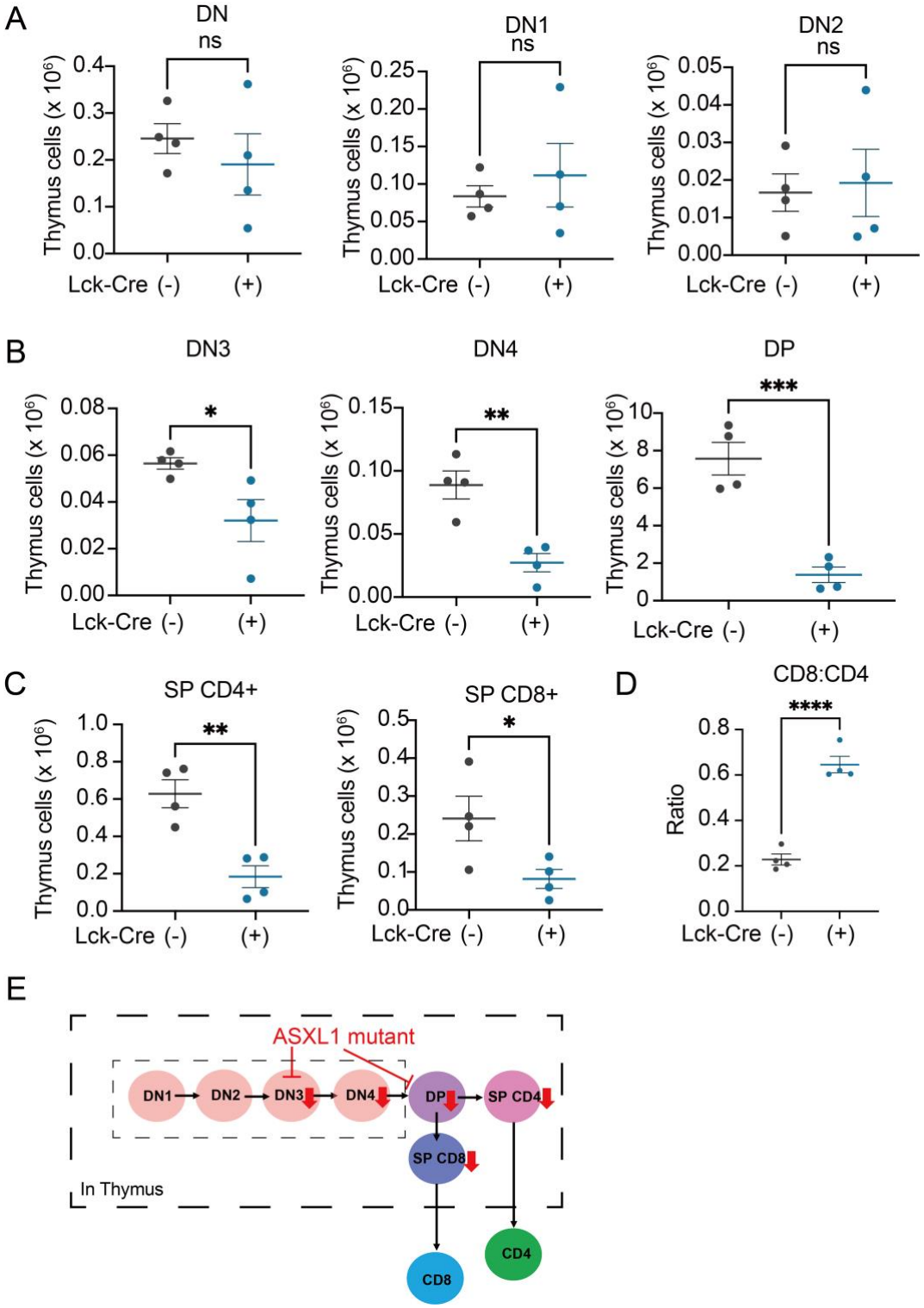
A
DN
ns
DN1
ns
DN2
ns
Thymus cells (x 10⁶)
Lck-Cre (-) (+)
B
DN3
*
DN4
**
DP
***
C
SP CD4+
**
SP CD8+
*
D
CD8:CD4
****
Ratio
E
ASXL1 mutant
DN1
DN2
DN3
DN4
DP
SP CD4
SP CD8
In Thymus
CD8
CD4

Figure 11. T cell development in Lck-Cre-*Asxl1*-KI-MT mice

A. The cell numbers of CD4-CD8- double negative (DN), DN1, DN2 fraction in thymus of Asxl1-MT$^{fl/fl}$ [Lck-Cre(-)] and Lck-Cre-Asxl1-MT$^{fl/fl}$ [Lck-Cre(+)] mice are shown is shown. **B**. The cell numbers of DN3, DN4 and CD4+CD8+ double positive (DP). **C**. The cell numbers of CD4+single positive (SP) and CD8+ SP fraction in thymus is shown. **D**. CD8/CD4 ratio in the peripheral blood of mice is shown. E. The scheme of the effect of mutant ASXL1 in T cell development in Lck-Cre-Asxl1-KI-MT. Data was shown in Mean ± SEM. Two tailed unpaired t test was performed for statistical analysis.

4.4 Asxl1-MT induces T-cell dysregulation in Vav-Cre-Asxl1-MT$^{fl/fl}$ mice

To examine the molecular changes in T cells expressing Asxl1-MT, I performed RNA-seq using splenocytes from control (Asxl1-MT$^{fl/fl}$) and Asxl1-MT (Vav-Cre-Asxl1-MT$^{fl/fl}$) mice. Hierarchical clustering revealed a clear separation between control and Asxl1-MT-expressing T cells (Figure 12A, B). MSigDB gene pathway overlap analysis revealed that Asxl1-MT upregulated genes related to IL-2-STAT5 signaling and inflammatory responses in both CD4$^+$ and CD8$^+$ T cells (Figure 12C, D). Activation of the IL-2-STAT5 pathway and upregulation of the pro-inflammatory genes indicate the chronic-activation and the exhaustion phenotype of Asxl1-MT-expressing T cells.

I previously showed that Asxl1-MT activates mitochondrial dysregulation as well as overproduction of ROS in HSCs(Fujino et al., 2021). Consistent with the phenotypes of Asxl1-MT expressing HSCs, I observed increased mitochondrial membrane potential in CD4$^+$ and CD8$^+$ Asxl1-MT expressing T cells (Figure 12E). Asxl1-MT also increased the intracellular ROS level in CD4$^+$ T cells and tended to increase it in CD8$^+$ T cells (Figure 12F). Collectively, these data suggest that Asxl1-MT provokes inflammation and mitochondrial dysregulation in T cells, thereby accelerating T cell aging.

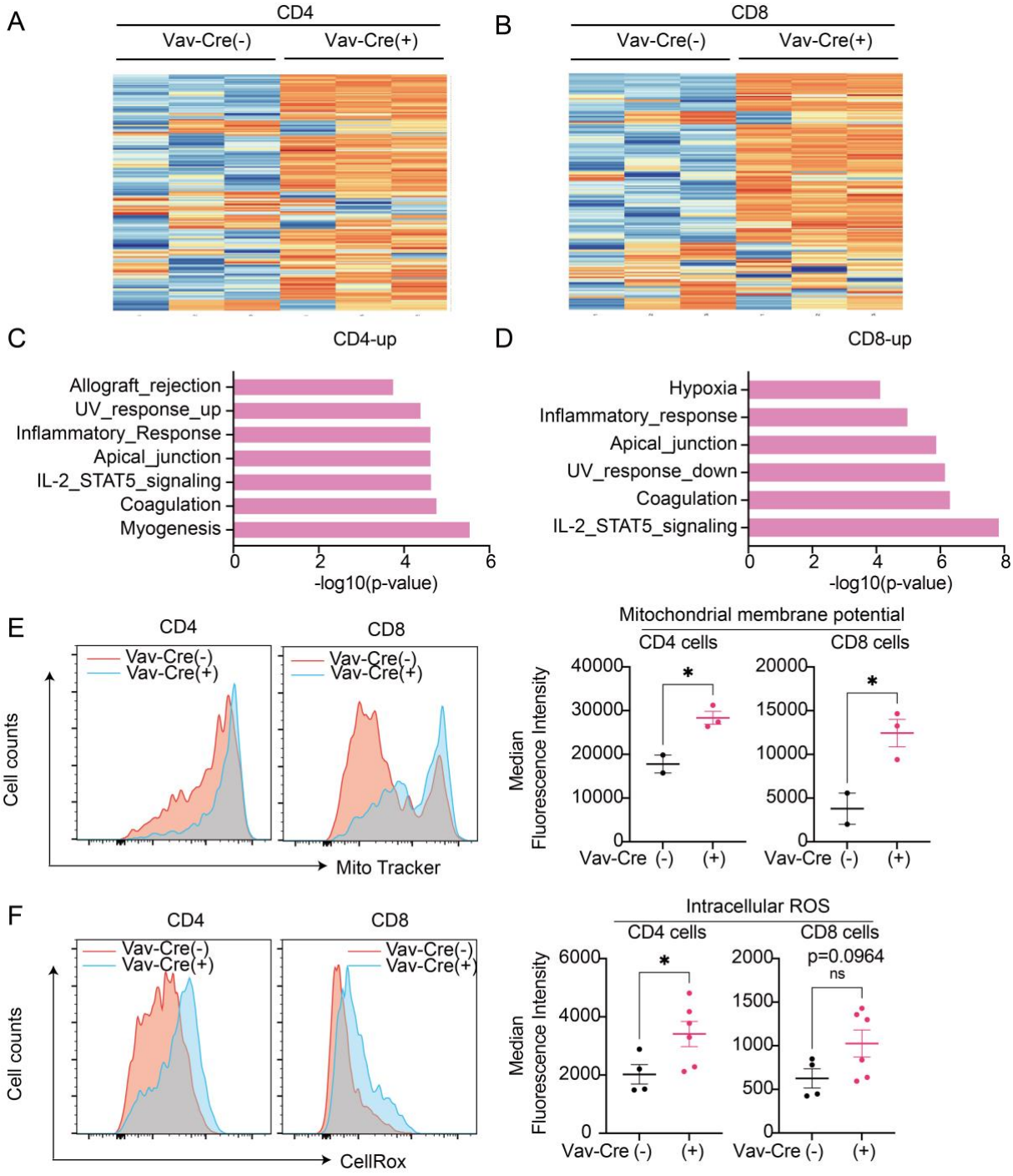
A
CD4
Vav-Cre(-)
Vav-Cre(+)
B
CD8
Vav-Cre(-)
Vav-Cre(+)
C
CD4-up
Allograft_rejection
UV_response_up
Inflammatory_Response
Apical_junction
IL-2_STAT5_signaling
Coagulation
Myogenesis
0
2
4
6
-log10(p-value)
D
CD8-up
Hypoxia
Inflammatory_response
Apical_junction
UV_response_down
Coagulation
IL-2_STAT5_signaling
0
2
4
6
8
-log10(p-value)
E
CD4
CD8
Vav-Cre(-)
Vav-Cre(+)
Cell counts
Mito Tracker
Mitochondrial membrane potential
CD4 cells
CD8 cells
Median Fluorescence Intensity
40000
30000
20000
10000
0
20000
15000
10000
5000
0
*
*
Vav-Cre (-)
(+)
F
CD4
CD8
Vav-Cre(-)
Vav-Cre(+)
Cell counts
CellRox
Intracellular ROS
CD4 cells
CD8 cells
Median Fluorescence Intensity
6000
4000
2000
0
2000
1500
1000
500
0
*
p=0.0964
ns
Vav-Cre (-)
(+)

Figure 12. Mutant ASXL1 induces inflammation and mitochondrial dysregulation in T cells

A-B. Hierarchical clustering of the RNA-Seq data of $CD4^+$ (**A**) and $CD8^+$(**B**) T cells. Top 200 genes most viable genes and comparison of control [Vav-Cre(-)] and Vav-Cre;Asxl1-$MT^{fl/fl}$ [Vav-Cre(+)] mice are shown. n = 3 per group. **C-D**. GSEA for up-regulated genes in **(C)** $CD4^+$ and **(D)** $CD8^+$ T cells using the MSigDB (http://software.broadinstitute.org/gsea/msigdb). The x-axis shows the P-value (－log10).

E. Mitochondrial membrane potential in $CD4^+$ and $CD8^+$ T cells of Asxl1-$MT^{fl/fl}$ [Vav-Cre(-)] (n=2) and Vav-Cre;Asxl1-$MT^{fl/fl}$ [Vav-Cre(+)](n=3). Representative histograms (left panel) and median fluorescence intensities (right panel) are shown. **F.** Intracellular ROS levels in in $CD4^+$ and $CD8^+$ T cells of Asxl1-$MT^{fl/fl}$ [Vav-Cre(-)] (n=4) and Vav-Cre;Asxl1-$MT^{fl/fl}$ [Vav-Cre(+)](n=6) mice. Representative histograms (left panel) and median fluorescence intensities (right panel) are shown. Data are shown as mean ± SEM. A two-tailed unpaired t-test was used for the comparison.

5. Discussion

In this study, I demonstrated that T cell-specific expression of Asxl1-MT promoted the growth of melanoma, lung cancer, and colon cancer cells in syngeneic models. Interestingly, this pro-tumor effect was not observed when Asxl1-MT was expressed in all hematopoietic lineage in Vav-Cre-Asxl1-MT$^{fl/fl}$ mice. These results suggest that myeloid cells or other immune cells with Asxl1-MT have anti-tumor functions that can diminish the pro-tumor effect of *ASXL1*-mutated T cells. However, T cell depletion or adoptive T-cell immunotherapy should be conducted to verify if T-cell is the only key factor in Asxl1-MT associated tumor environment. Indeed, I found that Asxl1-MT promotes a pro-inflammatory phenotype in monocytes and macrophages (Sato N et al., in submission), which are known to inhibit tumor progression. Thus, it is likely that Asxl1-MT-expressing immune cells have either pro- or anti-tumorigenic roles depending on the context and cell types. In addition to ASXL1, CHIP-associated TET2 mutations in immune cells were shown to modulate cancer progression. Previous studies have shown that TET2 depletion in myeloid cells alters T cell recruitment (Pan et al., 2017), (Li et al., 2020) and tumor angiogenesis(Nguyen et al., 2021). Interestingly, TET2 is also involved in maturation and activation of B cells, T cells and chimeric antigen receptor (CAR)-T cells (Li et al., 2021), (Jiang, 2020) ,(Fraietta et al., 2018) , indicating the potential role of

TET2-mutated lymphocytes in cancer development. Given the important roles of DNMT3A in myeloid and lymphoid cells (Cobo et al., 2022), DNMT3A-mutated immune cells may also be involved in the development of solid tumors. Further investigation will be required to determine the diverse roles of CHIP-associated mutations in immune cells and their impacts on solid tumor progression.

Importantly, Asxl1-MT promoted the development of spontaneous MMTV-PyMT-induced mammary tumors even in the Vav-Cre-Asxl1-MT$^{fl/fl}$ mice. The simultaneous development of the immune system with tumor likely leads to an immune tolerance environment in mice with anergic T cells compared with the syngeneic models (Guerin et al., 2020). This allows the MMTV-PyMT model to be more appropriate in terms of assessing the role of CH-associated ASXL1 in solid tumor progression. The correct microenvironment and longer latency period for tumor development in the MMTV-PyMT model may reveal the pro-tumor effect of the ASXL1 mutation in whole blood cells, which was not evident in the syngeneic transplantation models. The pro-tumor microenvironment was likely to be created by the reduction of infiltrated T cells and the exhaustion of $CD8^+$ T cells, but this should be confirmed experimentally using Lck-Cre-MMTV-PyMT-Asxl1-MT$^{fl/fl}$ mice in future studies. Because the Vav-Cre-Asxl1-MT$^{fl/fl}$ mice mimic many features of human CHIP, these results indicate that

somatic ASXL1 mutations in blood cells play a causal role in solid tumor progression probably through T cell dysregulation (see Summary). However, one limitation of our Vav-Cre-Asxl1-MT$^{fl/fl}$ mice is that Asxl1-MT is inserted after wildtype Asxl1 due to the Rosa26 knock in system, the observed phenotype may be bit stronger than the conventional Asxl1 mutations in human. Furthermore, it should be noted that all blood cells express Asxl1-MT in the Vav-Cre-Asxl1-MT$^{fl/fl}$ mice, while only a small fraction of blood cells have ASXL1 mutations in human CHIP carriers. Given that variant allele frequencies (VAFs) of most CHIP-associated mutations, including ASXL1 mutations, were higher in myeloid cells compared to lymphoid cells(Arends et al., 2018), whether the small numbers of T cells with ASXL1 mutations increase the risk of cancer in the long human life span remains unknown. The real contribution of CHIP clones in solid tumor development needs to be verified in spontaneous tumor models with small numbers of CHIP-cells.

Since *ASXL1* is frequently mutated in myeloid malignancies, diverse roles of Asxl1-MT in HSCs and myeloid cells have been rigorously investigated for the past few years(Asada et al., 2019),(Fujino and Kitamura, 2020). However, little was known about the role of Asxl1-MT in T cells. Our study revealed the unexpected effect of the ASXL1 mutation in the regulation of T cell development and function. In particular, Asxl1-MT

decreased naïve $CD4^+$ and $CD8^+$ T cell numbers, which is one of the hallmarks of aged T cells(Mittelbrunn and Kroemer, 2021). Asxl1-MT also induces upregulation of pro-inflammatory genes, mitochondrial dysregulation, and overproduction of the intracellular ROS in T cells. Because these phenotypes are often seen in aged T cells, Asxl1-MT may induce premature aging of T cells, as it does in HSCs (Fujino et al., 2021). It is also tempting to speculate that the altered T cell function may contribute to the evolution of ASXL1-CHIP and the development of myeloid neoplasms driven by ASXL1 mutations. However, there is not much clinical data on ASXL1 mutated blood cells in solid tumor patients, how ASXL1 mutations affect T cell development is still obscure and warrants further investigation in the clinic and the laboratory.

6. Summary

In summary, I showed that CHIP-associated Asxl1-MT induces T cell dysregulation and promotes tumor progression in multiple solid tumor models. Our findings raise the possibility that blood cells with ASXL1 mutations exacerbate solid tumor progression in ASXL1-CHIP carriers (Figure 13).

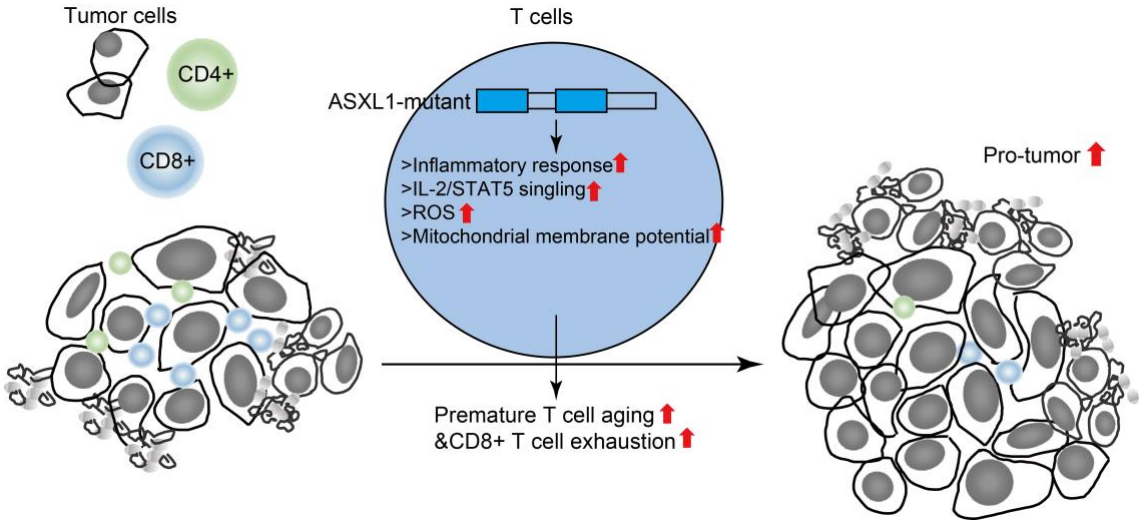

7. References

Abdel-Wahab, O., Adli, M., LaFave, L.M., Gao, J., Hricik, T., Shih, A.H., Pandey, S., Patel, J.P., Chung, Y.R., Koche, R., et al. (2012). ASXL1 Mutations Promote Myeloid Transformation through Loss of PRC2-Mediated Gene Repression. Cancer Cell *22*, 180–193.

Abdel-Wahab, O., Gao, J., Adli, M., Dey, A., Trimarchi, T., Chung, Y.R., Kuscu, C., Hricik, T., Ndiaye-Lobry, D., LaFave, L.M., et al. (2013). Deletion of Asxl1 results in myelodysplasia and severe developmental defects in vivo. J. Exp. Med. *210*, 2641–2659.

Aiello, A., Farzaneh, F., Candore, G., Caruso, C., Davinelli, S., Gambino, C.M., Ligotti, M.E., Zareian, N., and Accardi, G. (2019). Immunosenescence and Its Hallmarks: How to Oppose Aging Strategically? A Review of Potential Options for Therapeutic Intervention. Front. Immunol. *10*, 2247.

Arends, C.M., Galan-Sousa, J., Hoyer, K., Chan, W., Jäger, M., Yoshida, K., Seemann, R., Noerenberg, D., Waldhueter, N., Fleischer-Notter, H., et al. (2018). Hematopoietic lineage distribution and evolutionary dynamics of clonal hematopoiesis. Leukemia *32*, 1908–1919.

Asada, S., Goyama, S., Inoue, D., Shikata, S., Takeda, R., Fukushima, T., Yonezawa,

T., Fujino, T., Hayashi, Y., Kawabata, K.C., et al. (2018). Mutant ASXL1 cooperates with BAP1 to promote myeloid leukaemogenesis. Nat. Commun. *9*, 2733.

Asada, S., Fujino, T., Goyama, S., and Kitamura, T. (2019). The role of ASXL1 in hematopoiesis and myeloid malignancies. Cell. Mol. Life Sci. *76*, 2511–2523.

Balasubramani, A., Larjo, A., Bassein, J.A., Chang, X., Hastie, R.B., Togher, S.M., Lähdesmäki, H., and Rao, A. (2015). Cancer-associated ASXL1 mutations may act as gain-of-function mutations of the ASXL1–BAP1 complex. Nat. Commun. *6*, 7307.

Bejar, R., Stevenson, K., Abdel-Wahab, O., Galili, N., Nilsson, B., Garcia-Manero, G., Kantarjian, H., Raza, A., Levine, R.L., Neuberg, D., et al. (2011). Clinical Effect of Point Mutations in Myelodysplastic Syndromes. N. Engl. J. Med. *364*, 2496–2506.

de Boer, J., Williams, A., Skavdis, G., Harker, N., Coles, M., Tolaini, M., Norton, T., Williams, K., Roderick, K., Potocnik, A.J., et al. (2003). Transgenic mice with hematopoietic and lymphoid specific expression of Cre. Eur. J. Immunol. *33*, 314–325.

Bolton, K.L., Ptashkin, R.N., Gao, T., Braunstein, L., Devlin, S.M., Kelly, D., Patel, M., Berthon, A., Syed, A., Yabe, M., et al. (2020). Cancer therapy shapes the fitness landscape of clonal hematopoiesis. Nat. Genet. *52*, 1219–1226.

Clausen, B.E., Burkhardt, C., Reith, W., Renkawitz, R., and Förster, I. Conditional gene targeting in macrophages and granulocytes using LysMcre mice. 13.

Cobo, I., Tanaka, T., Glass, C.K., and Yeang, C. (2022). Clonal hematopoiesis driven by DNMT3A and TET2 mutations: role in monocyte and macrophage biology and atherosclerotic cardiovascular disease. Curr. Opin. Hematol. *29*, 1–7.

Cook, E.K., Izukawa, T., Young, S., Rosen, G., Jamali, M., Zhang, L., Johnson, D., Bain, E., Hilland, J., Ferrone, C.K., et al. (2019). Comorbid and inflammatory characteristics of genetic subtypes of clonal hematopoiesis. Blood Adv. *3*, 2482–2486.

Coombs, C.C., Zehir, A., Devlin, S.M., Kishtagari, A., Syed, A., Jonsson, P., Hyman, D.M., Solit, D.B., Robson, M.E., Baselga, J., et al. (2017). Therapy-Related Clonal Hematopoiesis in Patients with Non-hematologic Cancers Is Common and Associated with Adverse Clinical Outcomes. Cell Stem Cell *21*, 374-382.e4.

Corces-Zimmerman, M.R., Hong, W.-J., Weissman, I.L., Medeiros, B.C., and Majeti, R. Preleukemic mutations in human acute myeloid leukemia affect epigenetic regulators and persist in remission. CELL Biol. 6.

Cull, A.H., Snetsinger, B., Buckstein, R., Wells, R.A., and Rauh, M.J. (2017). Tet2 restrains inflammatory gene expression in macrophages. Exp. Hematol. *55*, 56-70.e13.

Davie, S.A., Maglione, J.E., Manner, C.K., Young, D., Cardiff, R.D., MacLeod, C.L., and Ellies, L.G. (2007). Effects of FVB/NJ and C57Bl/6J strain backgrounds on mammary tumor phenotype in inducible nitric oxide synthase deficient mice.

Transgenic Res. *16*, 193–201.

Fantozzi, A., and Christofori, G. (2006). Mouse models of breast cancer metastasis. Breast Cancer Res. *8*, 212.

Fraietta, J.A., Nobles, C.L., Sammons, M.A., Lundh, S., Carty, S.A., Reich, T.J., Cogdill, A.P., Morrissette, J.J.D., DeNizio, J.E., Reddy, S., et al. (2018). Disruption of TET2 promotes the therapeutic efficacy of CD19-targeted T cells. Nature *558*, 307–312.

Fujino, T., and Kitamura, T. (2020). ASXL1 mutation in clonal hematopoiesis. Exp. Hematol.

Fujino, T., Goyama, S., Sugiura, Y., Inoue, D., Asada, S., Yamasaki, S., Matsumoto, A., Yamaguchi, K., Isobe, Y., Tsuchiya, A., et al. (2021). Mutant ASXL1 induces age-related expansion of phenotypic hematopoietic stem cells through activation of Akt/mTOR pathway. Nat. Commun. *12*, 1826.

Fuster, J.J., MacLauchlan, S., Zuriaga, M.A., Polackal, M.N., Ostriker, A.C., Chakraborty, R., Wu, C.-L., Sano, S., Muralidharan, S., Rius, C., et al. (2017). Clonal hematopoiesis associated with TET2 deficiency accelerates atherosclerosis development in mice. 7.

Genovese, G., Kähler, A.K., Handsaker, R.E., Lindberg, J., Rose, S.A., Bakhoum, S.F., Chambert, K., Mick, E., Neale, B.M., Fromer, M., et al. (2014). Clonal Hematopoiesis

and Blood-Cancer Risk Inferred from Blood DNA Sequence. N. Engl. J. Med. *371*, 2477–2487.

Guerin, M.V., Finisguerra, V., Van den Eynde, B.J., Bercovici, N., and Trautmann, A. (2020). Preclinical murine tumor models: A structural and functional perspective. ELife *9*, e50740.

Guy, C.T., Cardiff, R.D., and Muller, W.J. (1992). Induction of mammary tumors by expression of polyomavirus middle T oncogene: a transgenic mouse model for metastatic disease. Mol. Cell. Biol. *12*, 954–961.

Inoue, D., Kitaura, J., Togami, K., Nishimura, K., Enomoto, Y., Uchida, T., Kagiyama, Y., Kawabata, K.C., Nakahara, F., Izawa, K., et al. (2013). Myelodysplastic syndromes are induced by histone methylationâ€“altering ASXL1 mutations. J. Clin. Invest. *123*, 4627–4640.

Jaiswal, S., and Ebert, B.L. (2019). Clonal hematopoiesis in human aging and disease. Science *366*, eaan4673.

Jaiswal, S., Fontanillas, P., Flannick, J., Manning, A., Grauman, P.V., Mar, B.G., Lindsley, R.C., Mermel, C.H., Burtt, N., Chavez, A., et al. (2014). Age-Related Clonal Hematopoiesis Associated with Adverse Outcomes. N. Engl. J. Med. *371*, 2488–2498.

Jaiswal, S., Natarajan, P., Silver, A.J., Gibson, C.J., Bick, A.G., Shvartz, E., McConkey,

M., Gupta, N., Gabriel, S., Ardissino, D., et al. (2017). Clonal Hematopoiesis and Risk of Atherosclerotic Cardiovascular Disease. N. Engl. J. Med. *377*, 111–121.

Jiang, S. (2020). Tet2 at the interface between cancer and immunity. Commun. Biol. *3*, 667.

Joseph, C., Quach, J.M., Walkley, C.R., Lane, S.W., Lo Celso, C., and Purton, L.E. (2013). Deciphering Hematopoietic Stem Cells in Their Niches: A Critical Appraisal of Genetic Models, Lineage Tracing, and Imaging Strategies. Cell Stem Cell *13*, 520–533.

Kaner, J., Desai, P., Mencia-Trinchant, N., Guzman, M.L., Roboz, G.J., and Hassane, D.C. (2020). Clonal Hematopoiesis and Premalignant Diseases. Cold Spring Harb. Perspect. Med. *10*, a035675.

Kim, D., Langmead, B., and Salzberg, S.L. (2015). HISAT: a fast spliced aligner with low memory requirements. Nat. Methods *12*, 357–360.

Lanzer, K.G., Johnson, L.L., Woodland, D.L., and Blackman, M.A. (2014). Impact of ageing on the response and repertoire of influenza virus-specific CD4 T cells. Immun. Ageing *11*, 9.

Li, J., Li, L., Sun, X., Deng, T., Huang, G., Li, X., Xie, Z., and Zhou, Z. (2021). Role of Tet2 in Regulating Adaptive and Innate Immunity. Front. Cell Dev. Biol. *9*, 665897.

Li, S., Feng, J., Wu, F., Cai, J., Zhang, X., Wang, H., Fetahu, I.S., Iwanicki, I., Ma, D.,

Hu, T., et al. (2020). TET 2 promotes anti-tumor immunity by governing G- MDSC s and CD 8 $^{+}$ T-cell numbers. EMBO Rep. *21*.

Liao, Y., Smyth, G.K., and Shi, W. (2019). The R package Rsubread is easier, faster, cheaper and better for alignment and quantification of RNA sequencing reads. Nucleic Acids Res. *47*, e47–e47.

Mittelbrunn, M., and Kroemer, G. (2021). Hallmarks of T cell aging. Nat. Immunol. *22*, 687–698.

Nagase, R., Inoue, D., Pastore, A., Fujino, T., Hou, H.-A., Yamasaki, N., Goyama, S., Saika, M., Kanai, A., Sera, Y., et al. (2018). Expression of mutant Asxl1 perturbs hematopoiesis and promotes susceptibility to leukemic transformation. J. Exp. Med. *215*, 1729–1747.

Nguyen, Y.T.M., Fujisawa, M., Nguyen, T.B., Suehara, Y., Sakamoto, T., Matsuoka, R., Abe, Y., Fukumoto, K., Hattori, K., Noguchi, M., et al. (2021). *Tet2* deficiency in immune cells exacerbates tumor progression by increasing angiogenesis in a lung cancer model. Cancer Sci. cas.15165.

Pan, W., Zhu, S., Qu, K., Meeth, K., Cheng, J., He, K., Ma, H., Liao, Y., Wen, X., Roden, C., et al. (2017). The DNA Methylcytosine Dioxygenase Tet2 Sustains Immunosuppressive Function of Tumor-Infiltrating Myeloid Cells to Promote

Melanoma Progression. Immunity *47*, 284-297.e5.

Rauch, P.J., Silver, A.J., Gopakumar, J., McConkey, M., Sinha, E., Fefer, M., Shvartz, E., Sukhova, G., Libby, P., Ebert, B.L., et al. (2018). Loss-of-Function Mutations in Dnmt3a and Tet2 Lead to Accelerated Atherosclerosis and Convergent Macrophage Phenotypes in Mice. Blood *132*, 745–745.

Ritchie, M.E., Phipson, B., Wu, D., Hu, Y., Law, C.W., Shi, W., and Smyth, G.K. (2015). limma powers differential expression analyses for RNA-sequencing and microarray studies. Nucleic Acids Res. *43*, e47–e47.

Robinson, M.D., McCarthy, D.J., and Smyth, G.K. (2010). edgeR: a Bioconductor package for differential expression analysis of digital gene expression data. Bioinformatics *26*, 139–140.

Saika, M., Inoue, D., Nagase, R., Sato, N., Tsuchiya, A., Yabushita, T., Kitamura, T., and Goyama, S. (2018). ASXL1 and SETBP1 mutations promote leukaemogenesis by repressing TGFβ pathway genes through histone deacetylation. Sci. Rep. *8*, 15873.

Sanchez, R., and Zhou, M.-M. (2011). The PHD finger: a versatile epigenome reader. Trends Biochem. Sci. S0968000411000491.

Scheuermann, J.C., de Ayala Alonso, A.G., Oktaba, K., Ly-Hartig, N., McGinty, R.K., Fraterman, S., Wilm, M., Muir, T.W., and Müller, J. (2010). Histone H2A

deubiquitinase activity of the Polycomb repressive complex PR-DUB. Nature *465*, 243–247.

Shlush, L.I., Zandi, S., Mitchell, A., Chen, W.C., Brandwein, J.M., Gupta, V., Kennedy, J.A., Schimmer, A.D., Schuh, A.C., Yee, K.W., et al. (2014). Identification of pre-leukaemic haematopoietic stem cells in acute leukaemia. Nature *506*, 328–333.

Takahama, Y., Ohishi, K., Tokoro, Y., Sugawara, T., Okabe, M., Kinoshita, T., and Takeda, J. Functional competence of T cells in the absence of glycosylphosphatidylinositol-anchored proteins caused by T cell-specific disruption of the Pig-agene. Eur J Immunol 8.

Uni, M., Masamoto, Y., Sato, T., Kamikubo, Y., Arai, S., Hara, E., and Kurokawa, M. (2019). Modeling ASXL1 mutation revealed impaired hematopoiesis caused by derepression of p16Ink4a through aberrant PRC1-mediated histone modification. Leukemia *33*, 191–204.

Yamamoto, K., Goyama, S., Asada, S., Fujino, T., Yonezawa, T., Sato, N., Takeda, R., Tsuchiya, A., Fukuyama, T., Tanaka, Y., et al. (2021). A histone modifier, ASXL1, interacts with NONO and is involved in paraspeckle formation in hematopoietic cells. Cell Rep. *36*, 109576.

Yang, H., Kurtenbach, S., Guo, Y., Lohse, I., Durante, M.A., Li, J., Li, Z., Al-Ali, H.,

Li, L., Chen, Z., et al. (2018). Gain of function of ASXL1 truncating protein in the pathogenesis of myeloid malignancies. Blood *131*, 328–341.

Youn, H.S., Kim, T.-Y., Park, U.-H., Moon, S.-T., An, S.-J., Lee, Y.-K., Hwang, J.-T., Kim, E.-J., and Um, S.-J. (2017). Asxl1 deficiency in embryonic fibroblasts leads to cellular senescence via impairment of the AKT-E2F pathway and Ezh2 inactivation. Sci. Rep. *7*, 5198.

Yu, G., Wang, L.-G., Han, Y., and He, Q.-Y. (2012). clusterProfiler: an R Package for Comparing Biological Themes Among Gene Clusters. OMICS J. Integr. Biol. *16*, 284–287.

Zhao, L., He, R., Long, H., Guo, B., Jia, Q., Qin, D., Liu, S.-Q., Wang, Z., Xiang, T., Zhang, J., et al. (2018). Late-stage tumors induce anemia and immunosuppressive extramedullary erythroid progenitor cells. Nat. Med. *24*, 1536–1544.

8. Acknowledgements

First and foremost, I would like to express my sincere gratitude to Prof. Toshio Kitamura for his passionate guidance for research and educational support in the lab. Next, I would like to sincerely thank my thesis advisor, prof. Susumu Goyama for the continuous support for my 3-years Ph.D. thesis. Prof. Goyama's patience, enthusiasm, and immense knowledge helped guide me all the time of my thesis research. I felt so honored to have Prof. Kitamura and Goyama as my mentors for my graduate school training at the University of Tokyo. Finally, I also want to express my sincere gratitude to the co-referees Prof. Iwama, and Prof. Hirata, for giving valuable advice through my 3-years Ph.D. Your kind support has enabled me to make progress for my project with a better vision and clearer direction.

I sincerely appreciate all the collaborators who were involved in my experiments, especially Prof. Takeharu Sakamoto, for providing research suggestions on my project, the solid tumor cells, and mouse models for my research. This project would be impossible without the help of Prof. Sakamoto. I also want to thank Prof. Yuji Yamanashi for proving the Lck-Cre mice and Prof. Yasunori Ota, Prof. Tamami Denda of the Department of Diagnostic Pathology, IMSUT for IHC analysis for MMTV-PyMT mice biopsies. I also thank the Flow Cytometry Core, the Mouse Core at IMSUT, for their help.

I sincerely thank Shiori Shikata for her expert technical assistance. In this project, mice genotyping is mandatory 2-3 times a month. The tumor tissue dissociation and tumor infiltrated immune cells analysis costs a long time (it will cost consecutively 16 hours if I do all the processes alone). Without her assistance, this project will be very difficult to do. I also want to thank Dr. Takeshi Fujino, Dr. Naru Sato, and Ms. Yuko Shimosato for their assistants on ASXL1-MT mice studies, especially Dr. Naru Sato, for advised me on LysM-Cre and monocytes analysis, Ms. Yuko Shimosato for T cell analysis.

Finally, I would like to express my profound gratitude to my family and to my other lab colleges at the Division of Cell Therapy and Division of Molecular Oncology, the University of Tokyo for providing me with unfailing support and continuous encouragement through the process of researching and writing this thesis paper. This accomplishment would not have been possible without all of you. Thank you.